

Federated Causal Representation Learning in State-Space Systems for Decentralized Counterfactual Reasoning

Nazal Mohamed^{*1}

Ayush Mohanty^{*1}

Nagi Gebraeel¹

¹Georgia Institute of Technology, Atlanta, GA

Abstract

Networks of interdependent industrial assets (clients) are tightly coupled through physical processes and control inputs, raising a key question: *how would the output of one client change if another client were operated differently?* This is difficult to answer because client-specific data are high-dimensional and private, making centralization of raw data infeasible. Each client also maintains proprietary local models that cannot be modified. We propose a federated framework for causal representation learning in state-space systems that captures interdependencies among clients under these constraints. Each client maps high-dimensional observations into low-dimensional latent states that disentangle intrinsic dynamics from control-driven influences. A central server estimates the global state-transition and control structure. This enables decentralized counterfactual reasoning where clients predict how outputs would change under alternative control inputs at others while only exchanging compact latent states. We prove convergence to a centralized oracle and provide privacy guarantees. Our experiments demonstrate scalability, and accurate cross-client counterfactual inference on synthetic and real-world industrial control system datasets.

1 INTRODUCTION

Complex industrial systems such as oil refineries, water treatment networks, and distributed process plants consist of geographically dispersed yet tightly coupled assets (clients) that interact dynamically through control actions and material flows. A change at one client such as a pump adjustment or valve operation, can causally propagate to others, influ-

encing both performance and safety across the network. These interdependencies make the system vulnerable to cascading disruptions, where local disturbances can escalate into large-scale operational failures Pournaras et al. [2020], Ghosh et al. [2025]. Managing these risks requires causal models that not only identify which clients influence one another, but also reason about how interventions propagate across the system.

Granger causality (GC) is a classical tool for detecting interdependencies in time-series data Granger [1969], Geweke [1982], Tang et al. [2023]. Yet GC is fundamentally predictive rather than interventional, and thus **cannot** answer counterfactual questions such as: *how would my output have changed if another client had altered its control input?* Moreover, GC conflates intrinsic state dynamics with control-driven influences, leaving the source of interdependencies ambiguous.

In practice, however, operators often need exactly this type of counterfactual reasoning Tang et al. [2023], Ruiz-Tagle et al. [2022]. For instance, assessing “*how reducing flow at an upstream unit would affect downstream stability*”, or “*how adjusting a peer’s control settings might influence local product quality*”. Without such capabilities, decision-making remains limited to retrospective diagnostics rather than proactive intervention planning. Practical constraints further complicate this problem. Modern assets generate high-dimensional sensor data that is expensive to transmit, while bandwidth and communication limits prevent centralization. Privacy regulations and confidentiality concerns restrict data sharing across organizational boundaries. Finally, each client typically maintains a proprietary local model trained on its own data, which must remain intact and cannot be altered in a data analysis pipeline. To address these challenges, we develop a federated learning framework tailored to distributed industrial systems.

Contributions. We focus on linear state-space systems, which provide a tractable representation of causally interdependent dynamics using low-dimensional latent states. In

^{*}Equal contribution.

our framework, each client retains its proprietary model and maps raw high-dimensional measurements into disentangled low-dimensional latent states. Specifically, at the client level, we utilize a modeling approach that separates autoregressive time-series dynamics from control effects. A central server acting as a conduit between these interdependent clients estimates the global structures for the state-transition and input matrices without direct access to raw high-dimensional data (measurements). This architecture equips each client to answer counterfactual queries, such as predicting how its outputs would change if another client altered its controls without sharing raw data, inputs, or proprietary models. To the best of our knowledge, this is the first work to enable decentralized counterfactual reasoning. The key technical contributions of this paper are as follows:

- We employ the “*Abduction-Action-Prediction*” framework of Pearl [2009] to formally derive the average treatment effect in the federated setting, enabling decentralized counterfactual reasoning.
- We propose a federated learning approach in which the server explicitly estimates the state-transition and input matrices, while clients learn their implicit effects, without moving any private, high-dimensional data.
- We design an iterative optimization scheme across servers and clients that provably disentangles autoregressive dynamics from exogenous inputs, a key requirement for decentralized counterfactual reasoning.
- We prove convergence of the decentralized framework to a centralized oracle with direct access to all high-dimensional client measurements. In addition, we provide differential privacy guarantees for the federated protocols by quantifying the perturbations required in communicated quantities to protect client data.
- Experiments on synthetic data validate the main claims of the paper w.r.t. counterfactual reasoning, convergence to a centralized oracle, and differential privacy, and further demonstrate robustness and scalability. Real-world experiments confirm the applicability of the approach of industrial control systems.

2 RELATED WORK

Causal Inference in Dynamical Systems. Granger causality (GC) is the classical tool for detecting predictive dependencies in time series Granger [1969], Geweke [1982], Barnett et al. [2009]. Extensions such as structural GC Eichler [2010] and causal state-space models Huang et al. [2019], Mastakouri et al. [2021] have attempted to incorporate interventional semantics, but they typically assume centralized access and conflate endogenous dynamics with exogenous inputs. Probabilistic approaches including dynamic Bayesian networks Murphy [2002] and latent-variable state-space models Krishnan et al. [2015], Fraccaro et al. [2017]

improve representation power but remain predictive in nature.

Federated Causal Discovery. Federated learning McMahan et al. [2017] has been extended to causal discovery across distributed clients. Li et al. [2024b] propose federated conditional independence testing for heterogeneous data. Mian et al. [2022, 2023] introduce regret-based methods with privacy guarantees. FedECE Ye et al. [2024] estimates causal effects across institutions using graphical modeling without data sharing. Zhao et al. [2025] develop a distributed annealing algorithm for federated DAG learning under generalized linear models, offering identifiability guarantees. More recent works address scalability. FedCausal Yang et al. [2024] unifies local and global optimization through adaptive strategies, while FedCSL Guo et al. [2024] improves accuracy with local-to-global learning and weighted aggregation. Despite these advances, existing methods focus on structural recovery or associations. They lack counterfactual semantics.

Causal Representation Learning. Pearl’s Abduction–Action–Prediction (AAP) framework Pearl [2009] formalizes counterfactual inference and underpins modern causal reasoning. Extensions such as invariant causal prediction Peters et al. [2016], invariant risk minimization Arjovsky et al. [2019], and causal representation learning Schölkopf et al. [2021], Brehmer et al. [2022], Lippe et al. [2022] aim to learn invariant and intervention-aware representations. Disentangled state-space models Miladinović et al. [2019], Weng et al. [2025], and disentangled representation learning Li et al. [2024a], Wang et al. [2024] improve interpretability but assume centralized data access. Recent counterfactual time-series approaches like Mastakouri et al. [2021], Todo et al. [2023] also remain centralized.

3 PRELIMINARIES

Linear Time Invariant (LTI) Systems. The dynamics of a linear system can be described by the following LTI state-space equations:

$$h^t = A h^{t-1} + B u^{t-1} + w^{t-1}; y^t = C h^t + v^t, \quad (1)$$

where $h^t \in \mathbb{R}^P$ is the latent state, $u^t \in \mathbb{R}^S$ is the input (or control), and $y^t \in \mathbb{R}^D$ is the measurement (also called observation or output). The matrices $A \in \mathbb{R}^{P \times P}$, $B \in \mathbb{R}^{P \times S}$, and $C \in \mathbb{R}^{D \times P}$ are time-invariant state-transition, input, and output matrices, respectively. $w^{t-1} \sim \mathcal{N}(0, Q_w)$, and $v^t \sim \mathcal{N}(0, R_v)$ are the process noise and measurement noise, respectively.

Structural Causal Models (SCMs). In a causal system, we represent interdependencies among variables using a *causal graph*, where nodes correspond to variables and directed edges encode direct causal influence. For any vari-

able X , we denote by $\text{Pa}(X)$ the set of its parent nodes. We then distinguish between two types of variables: **(1) Exogenous variables (U)** are determined outside the system being modeled. They capture background factors, noise, or unobserved influences not explained by the model itself. **(2) Endogenous variables (H)** are determined within the system by structural equations. Structural assignments E generate each endogenous variable H from its parents $\text{Pa}(H)$ in the causal graph and an associated exogenous variable U such that, $H := E(\text{Pa}(H), U)$. A structural causal model (SCM) specifies an ordered triplet $\langle U, H, E \rangle$, providing a principled way to infer causal relationships in a system.

Intervention. An intervention, denoted by $\text{do}(u = u')$, $u \in U$, is an experiment performed by replacing the structural assignment of u with the constant u' and leaving all other assignments unchanged. Pearl [2009]’s Abduction-Action-Prediction (AAP) scheme given below, provides a principled approach to infer the consequence of intervention:

1. **Abduction:** infer latent quantities from past observations
2. **Action:** encode the intervention by modifying the relevant structural assignment(s)
3. **Prediction:** propagate the intervened model forward to obtain interventional outcomes.

Predicting the consequence of intervention is the key to answering counterfactual questions such as, “*what would $h \in H$ have been under a different value of u ?*”. A common way to quantify such effects is via the *average treatment effect* (ATE), defined as follows:

$$ATE := \mathbb{E}[h \mid \text{do}(u = u_1)] - \mathbb{E}[h \mid \text{do}(u = u_0)], \quad (2)$$

In other words, ATE measures the expected change in the endogenous variable h when the exogeneous variable u is set to u_1 instead of u_0 through intervention.

LTI system as an SCM. The LTI state-space system in (1) can be alternatively viewed as an SCM, where h^t and y^t are endogenous variables, and u^{t-1} , w^t and v^t are exogenous. The input u^{t-1} is not governed by the system dynamics but externally specified. Hence u^{t-1} qualifies as an intervention variable. The state h^t **cannot** be observed directly (thus, called *latent state*) and has to be estimated from the measurements y^t , using a Kalman filter Kalman [1960].

4 COUNTERFACTUALS FOR LTI

Proposition 4.1. *Let the input to an LTI system be $u^{t-1} = u_0$. Then the ATE on measurements y^t under the intervention $\text{do}(u^{t-1} = u_1)$ equals $CB(u_1 - u_0)$.*

Proposition 4.1 shows that only the matrices C and B parameterize the ATE of externally applied inputs u on downstream measurements y .

4.1 MULTI-CLIENT SYSTEM

We consider a *multi-client* LTI state-space setting with M clients (subsystems). Client $m \in \{1, \dots, M\}$ has local state $h_m^t \in \mathbb{R}^{P_m}$, input $u_m^t \in \mathbb{R}^{U_m}$, and measurement $y_m^t \in \mathbb{R}^{D_m}$, with $D_m \gg P_m, U_m$. The joint dynamics follow Eq (1). We further assume:

Assumption 4.2. The matrix C is block-diagonal.

Rationale. In many engineered systems, sensors are tied to a physical subsystem, so y_m^t depends **only** on h_m^t , i.e., $y_m^t = C_{mm}h_m^t$.

Under Assumption 4.2, Proposition 4.1 gives the following causal effect (ATE) in the multi-client setting:

$$\begin{aligned} \mathbb{E}[y_m^t \mid \text{do}(u_n^{t-1} = u_{n_1})] - \mathbb{E}[y_m^t \mid \text{do}(u_n = u_{n_0})] \\ = C_{mm}B_{mn}(u_{n_1} - u_{n_0}) \quad \forall m \neq n \end{aligned} \quad (3)$$

Equation 3 addresses the **counterfactual** query:

Q1. “*What would y_m^t have been if client n ’s input u_n^{t-1} had changed?*”

Problem Formulation. We study counterfactual reasoning in multi-client LTI systems under decentralized constraints. Each client observes only high-dimensional local measurements y_m^t , with no access to other clients’ data. The goal is to estimate cross-client causal effects B_{mn} (Eq. 3) that answer **Q1**, while respecting privacy and comm. constraints.

Role of A in Latent-State Recovery. Although the ATE in Proposition 4.1 depends only on B_{mn} , estimating it in practice requires access to latent states h^t . These states evolve according to the transition matrix A . Without modeling A , one cannot disentangle **(i)** endogenous propagation of past states via A_{mn} from **(ii)** exogenous input effects via B_{mn} . Thus, learning $A_{mn} \forall m, n$ is essential both for recovering h^t and for isolating the causal contribution of B_{mn} .

4.2 DECENTRALIZED SETTING

While Eq. 3 identifies B_{mn} as the key parameter for counterfactual reasoning, estimating it in a decentralized environment is challenging due to: **(1) Partial observability:** Only noisy measurements y^t are observed locally. Recovering B_{mn} requires first inferring latent states h^t by modeling A and then separating the effects of A_{mn} and B_{mn} . **(2) Data sharing constraints:** Clients cannot share raw y^t due to privacy, and y^t is often high-dimensional, making direct communication infeasible.

These constraints motivate a federated approach to estimate $\{A_{mn}, B_{mn}\}$. Each client transmits low-dimensional state estimates \hat{h}_m^t , and inputs u_m^t to a coordinating server, without exposing raw measurements y_m^t . The server explicitly estimates $\{A_{mn}, B_{mn}\}$ using aggregated $\{\hat{h}^t, u^t\}$ across

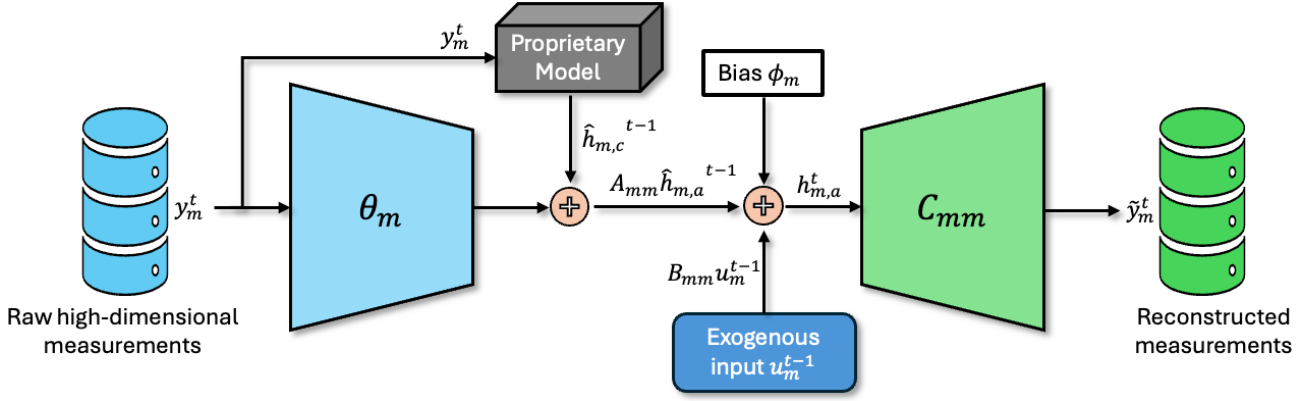


Figure 1: A simplified view of the computation inside the client m

clients (extending prior work, e.g., Mohanty et al. [2025], which solved only the special case $B \equiv 0$). This enables server-side counterfactual reasoning via Eq. 3.

Key challenge for clients. Unlike the server, client m observes only its own \hat{h}_m^t and u_m^t , and receives no states or inputs from others. Local estimates, therefore, conflate two sources of variation: **(i)** endogenous propagation of past states (through A_{mm}) and **(ii)** exogenous input effects (through B_{mm}). To support **Q1** locally, clients must learn representations in which these effects are **disentangled**, so that B_{mm} can be isolated and used in Eq. 3. Our training methodology is designed to enforce this disentanglement at the client, while relying only on server communications.

5 FEDERATED TRAINING

5.1 PROPRIETARY CLIENT MODEL

Assumption 5.1. Each client m knows its local block matrices A_{mm} , B_{mm} , and C_{mm} .

Rationale. The matrices A_{mm} , B_{mm} , and C_{mm} correspond to the diagonal blocks of the global state-transition matrix A , input matrix B , and output matrix C of the LTI system. These local blocks do not affect counterfactual query **Q1**. Moreover, if not pre-specified, they can be readily estimated by each client using only its own data.

Notation. Kalman filtering distinguishes a one-step-ahead *predicted state* from a *refined estimated state*. We denote by h^t the one-step-ahead prediction at time t (based on information up to $t-1$), and by \hat{h}^t the refined estimate after observing y^t at time t .

The proprietary client model is a Kalman filter (in general it can be any state estimator), which makes use of the local block matrices A_{mm} , B_{mm} , C_{mm} , the local measurement y_m^t , and input u_m^t to compute a *predicted state* $h_{m,c}^t$ and a *refined estimate* $\hat{h}_{m,c}^t$.

Assumption 5.2. The proprietary model provides both $h_{m,c}^t$ (predicted state) and $\hat{h}_{m,c}^t$ (refined estimate), which are treated as given inputs to our federated learning method.

Limitation of the Proprietary Model. Since the proprietary model relies exclusively on local information (i.e., A_{mm} , B_{mm} , C_{mm} , y_m^t , and u_m^t), it **cannot** capture cross-client interdependencies and is therefore unable to answer query **Q1** (Section 4.2).

5.2 AUGMENTED CLIENT MODEL

To overcome the limitations of the proprietary model, we **augment** it with additional ML parameters, yielding an *augmented client model*. The governing equations are:

$$h_{m,a}^t = A_{mm} \hat{h}_{m,a}^{t-1} + B_{mm} u_m^{t-1} + \phi_m, \quad (4)$$

$$\hat{h}_{m,a}^t = \hat{h}_{m,c}^t + \theta_m y_m^t. \quad (5)$$

Here, $h_{m,a}^t$ denotes the *augmented predicted state*, and $\hat{h}_{m,a}^t$ the *augmented refined estimate*, which extends the proprietary estimate $\hat{h}_{m,c}^t$ by incorporating the learned parameter θ_m . The corresponding **client loss** is defined as, $L_{m,a}^t := \|r_{m,a}^t\|_2^2$, where we have,

$$r_{m,a}^t = y_m^t - \tilde{y}_{m,a}^t, \quad \text{with} \quad \tilde{y}_{m,a}^t = C_{mm} h_{m,a}^t. \quad (6)$$

Therefore, the client loss is just a *reconstruction loss* with $\tilde{y}_{m,a}^t$ denoting the *reconstructed measurement*, which serves as the key output for counterfactual analysis (used later in Section 6).

Parameter updating. Each client updates ϕ_m and θ_m by combining gradients from its own loss $L_{m,a}$ with gradients derived from the **server loss** L_s . Importantly, the server never sends raw data; instead, it communicates only the gradients with respect to the augmented states, namely $\nabla_{h_{m,a}^t} L_s$ and $\nabla_{\hat{h}_{m,a}^{t-1}} L_s$. The client then uses the chain rule of partial derivatives (proof can be found in the Appendix)

to compute:

$$\nabla_{\theta_m} L_s = \sum_{t=1}^T \left(A_{mm}^\top \cdot \nabla_{h_{m,a}^t} L_s + \nabla_{\hat{h}_{m,a}^{t-1}} L_s \right) y_m^{t-1 \top} \quad (7)$$

$$\nabla_{\phi_m} L_s = \sum_{t=1}^T \nabla_{h_{m,a}^t} L_s. \quad (8)$$

Using the locally computed $\nabla_{\theta_m} L_s$, $\nabla_{\phi_m} L_s$, and learning rates $\eta_1, \eta_2, \gamma_1, \gamma_2$, the updated parameters are then given by,

$$\theta_m^{k+1} = \theta_m^k - \eta_1 \nabla_{\theta_m} L_{m,a} - \eta_2 \nabla_{\theta_m} L_s, \quad (9)$$

$$\phi_m^{k+1} = \phi_m^k - \gamma_1 \nabla_{\phi_m} L_{m,a} - \gamma_2 \nabla_{\phi_m} L_s. \quad (10)$$

Claim 5.3. The local client parameters θ_m and ϕ_m learn to encode cross-client interdependencies arising from off-diagonal blocks A_{mn} and B_{mn} ($n \neq m$).

Intuition on Claim 5.3. Although each client observes only local data, the server gradients $\nabla_{\theta_m} L_s$ and $\nabla_{\phi_m} L_s$ implicitly carry information about how other clients' data influence the server loss. When combined with local gradients, these updates guide θ_m and ϕ_m to represent cross-client effects, enabling the augmented model to capture interdependencies that the proprietary model cannot. A theoretical proof is provided in Section 6, with empirical validation in Section 9.

Comm. to the Server: Each client m sends $\{\hat{h}_{m,c}^t, \hat{h}_{m,a}^t, h_{m,a}^t, u_m^t\}$ to the server.

5.3 SERVER MODEL

Assumption 5.4. The diagonal blocks A_{mm} and B_{mm} are known at the server.

Rationale behind Assumption 5.4. From Assumption 5.1, each client m already has access to A_{mm} and B_{mm} . Their effects are purely local and do not influence cross-client counterfactual reasoning, hence they are not central to our analysis. Communicating them to the server, therefore, incurs only a fixed one-time cost during initialization.

After receiving $\hat{h}_{m,c}^t, \hat{h}_{m,a}^t, h_{m,a}^t$, and u_m^t from client m , together with the known diagonal blocks $\{A_{mm}, B_{mm}\}$ and the current estimates of $\{\hat{A}_{mn}, \hat{B}_{mn}\}_{n \neq m}$, the server predicts the future state $h_{m,s}^t$, and computes a residual $r_{m,s}^t$ given by,

$$h_{m,s}^t = A_{mm} \hat{h}_{m,c}^{t-1} + \sum_{n \neq m} \hat{A}_{mn} \hat{h}_{n,c}^{t-1} + B_{mm} u_m^{t-1} + \sum_{n \neq m} \hat{B}_{mn} u_n^{t-1}, \quad \text{and} \quad (11)$$

$$r_{m,s}^t = h_{m,s}^t - h_{m,a}^t. \quad (12)$$

To learn an estimate of the off-diagonal blocks $\{A_{mn}, B_{mn}\}_{n \neq m}$, the server minimizes a loss,

$$L_s := \frac{1}{T} \sum_{t=1}^T \sum_{m=1}^M \left(\|r_{m,s}^t\|_2^2 + \xi_m \underbrace{\|A_{mm} (\hat{h}_{m,a}^{t-1} - \hat{h}_{m,c}^{t-1}) - \sum_{n \neq m} \hat{A}_{mn} \hat{h}_{n,c}^{t-1}\|_2^2}_{\mathcal{D}} \right) \quad (13)$$

Claim 5.5. With large ξ_m , \mathcal{D} disentangles cross-client effects of A_{mn} (endogenous) and B_{mn} (exogenous).

Claim 5.5 ensures that each client separates the contributions of A_{mn} and B_{mn} when learning its parameters θ_m and ϕ_m , respectively. Theoretical proof of Claim 5.5 is provided in Section 6.

Parameter Updating. The server updates the off-diagonal blocks by block gradient descent,

$$\hat{A}_{mn}^{k+1} = \hat{A}_{mn}^k - \alpha_A \nabla_{\hat{A}_{mn}^k} L_s, \quad \text{and} \quad (14)$$

$$\hat{B}_{mn}^{k+1} = \hat{B}_{mn}^k - \alpha_B \nabla_{\hat{B}_{mn}^k} L_s, \quad \forall n \neq m. \quad (15)$$

Comm. to the Clients. The server communicates gradients $\nabla_{h_{m,a}^t} L_s$ to each client m .

5.4 OVERHEAD

Communication. At each training round, every client transmits latent states and inputs $\{\hat{h}_{m,c}^t, \hat{h}_{m,a}^t, h_{m,a}^t, u_m^t\}$ of dimension $\mathcal{O}(P_m + U_m)$ to the server, and receives gradient updates of size $\mathcal{O}(P_m)$, leading to a per-round communication cost of $\mathcal{O}(M(P + U))$, where $P = \sum_m P_m$ and $U = \sum_m U_m$.

Computation. The server performs block gradient descent over matrices $\{A_{mn}, B_{mn}\}$, with per-round complexity $\mathcal{O}(M^2 P^2 + M^2 U^2)$ in the worst case. Each client's local updates (Eqs. 10) require $\mathcal{O}(T P_m^2)$ operations per round, dominated by matrix-vector products with dimension P_m .

6 CAUSAL REPRESENTATIONS

The training in Section 5 is iterative: **(i)** the server learns cross-client dependencies via off-diagonal blocks A_{mn}, B_{mn} ($n \neq m$), and **(ii)** clients encode them in local parameters θ_m, ϕ_m . Cross-client information flows to the server through low-dimensional states, and to clients via server-loss gradients L_s (Claim 5.3). We now show these gradients explicitly encode A_{mn}, B_{mn} :

The gradients sent from the server to the client m are

$\nabla_{h_{m,a}^t} L_s$ defined as,

$$\nabla_{h_{m,a}^t} L_s := \frac{2}{T} \left(h_{m,a}^t - [A_{mm} \hat{h}_{m,c}^{t-1} + \sum_{n \neq m} \hat{A}_{mn} \hat{h}_{n,c}^{t-1} + B_{mm} u_m^{t-1} + \sum_{n \neq m} \hat{B}_{mn} u_n^{t-1}] \right). \quad (16)$$

Eq. 16 shows that $\nabla_{h_{m,a}^t} L_s$ depends on both A_{mn} and B_{mn} . By Eqs. 8–10, θ_m and ϕ_m thus learn an **entangled representation** of these effects. Yet counterfactuals in Eq. 3 require isolating B_{mn} from A_{mn} , making entanglement a barrier to answering query **Q1**. The next section addresses disentanglement via Claim 5.5.

For all clients m , at any time t , the following hold:

Theorem 6.1. *In Eq. 13, as $\xi \rightarrow \infty$, the stationary points \hat{A}_{mn}^* of the server and θ_m^* of the clients satisfy*

$$\mathbb{E} \left[A_{mm} \theta_m^* y_m^t \right] = \mathbb{E} \left[\sum_{n \neq m} \hat{A}_{mn}^* \hat{h}_{n,c}^t \right] \quad \forall m \neq n. \quad (17)$$

Corollary 6.2. *As $\xi \rightarrow \infty$, the stationary points B_{mn}^* of the server and ϕ_m^* of the clients satisfy*

$$\phi_m^* = \mathbb{E} \left[\sum_{n \neq m} \hat{B}_{mn}^* u_n^t \right] \quad \forall m \neq n. \quad (18)$$

With sufficiently large ξ_m (Eq. 13), Theorem 6.1 and Corollary 6.2 ensure client parameters disentangle A_{mn} and B_{mn} , even though the server communicated gradients $\nabla_{h_{m,a}^t} L_s$ remain entangled (Eq. (16)).

We have established that the client m implicitly learns $\sum_{n \neq m} B_{mn} u_n^t$ (in expectation) through its augmented parameter ϕ_m , while the server explicitly learns B_{mn} for all $n \neq m$. Consequently, both can answer counterfactual queries, albeit with different fidelity:

(1) Server. The server evaluates counterfactuals at the state level, estimating the following quantity:

$$\mathbb{E}[h_{m,s}^t \mid \text{do}(u_n^{t-1} = u_{n_1})] - \mathbb{E}[h_{m,s}^t \mid \text{do}(u_n^{t-1} = u_{n_0})] = B_{mn}(u_{n_1} - u_{n_0}), \quad (19)$$

answering: **Q2.** “What would $h_{m,s}^t$ have been if client n ’s input u_n^{t-1} had changed?”

(2) Client. The client evaluates counterfactuals at the measurement level, essentially estimating:

$$\begin{aligned} & \mathbb{E}[\tilde{y}_{m,a}^t \mid \text{do}(\phi_m = \phi_{m_1})] - \mathbb{E}[\tilde{y}_{m,a}^t \mid \text{do}(\phi_m = \phi_{m_0})] \\ &= C_{mm}(\phi_{m_1} - \phi_{m_0}), \\ &= C_{mm} \cdot \mathbb{E} \left[\sum_{n \neq m} B_{mn}(u_{n_1} - u_{n_0}) \right] \end{aligned} \quad (20)$$

which, by Corollary 6.2, answers the query:

Q3. “What would $\tilde{y}_{m,a}^t$ have been if the aggregated effects of inputs from other clients had changed?”

Thus, the server isolates the effect of a specific client’s input u_n , while the client reasons only through the aggregated influence $\sum_{n \neq m} B_{mn} u_n$ encoded in ϕ_m .

6.1 CAUSAL IDENTIFIABILITY

A central question in causal representation learning is whether a model has truly learned the underlying causal structure or has merely fit the observed data. Ideally, one would verify that the server learned parameters \hat{A}_{mn} and \hat{B}_{mn} match the ground-truth structural parameters $(A_m n, B_m n)$. However, this comparison is complicated by a fundamental identifiability issue: The structural parameters of an LTI system are **not** uniquely recoverable from input u and measurements y (also called *input-output* data).

For example, if the latent state h_m^t is reparameterized by any invertible transformation T as $h'_t = Th_t$, then the triple $(A' = TAT^{-1}, B' = TB, C' = CT^{-1})$ defines a different-looking set of structural matrices that generates identical observations y^t . Consequently, different parameterizations of (A, B, C) are all equally consistent with the input-output data. This makes a direct comparison of learned parameters to a specific ground-truth realization, an ill-posed criterion.

That brings us to the important question: *What is uniquely determined by the input-output data?* That quantity is the *transfer function* $G(z) = C(zI - A)^{-1}B$, which encodes how interventions on u^t propagate to measurements y^t . Given the representation of LTI systems as SCMs discussed in Sections 3 and 4, the **transfer function is precisely the object that carries causal meaning**. It is invariant to basis changes in the latent state and uniquely determines the ATE of Proposition 4.1. Our framework implicitly learns this transfer function $G(z)$ without any data centralization.

7 PRIVACY ANALYSIS

We provide theoretical results on the differential privacy analysis of the proposed framework in the Appendix 11.

8 CONVERGENCE TO AN ORACLE

We consider a centralized model as the *oracle* for our approach. Since each proprietary client model is a local Kalman filter (KF), a natural oracle that encodes full cross-client causality is a centralized KF with access to all clients’ data and full knowledge of (A, B) . Thus the oracle’s dynamics are governed as:

$$h_o^t = A \hat{h}_o^{t-1} + B u^{t-1}; \quad \tilde{y}_o^t = C h_o^t, \quad (21)$$

$$r_o^t = y^t - \tilde{y}_o^t; \quad \text{and} \quad \hat{h}_o^t = h_o^t + K_o^t r_o^t, \quad (22)$$

where K_o^t is the centralized Kalman gain.

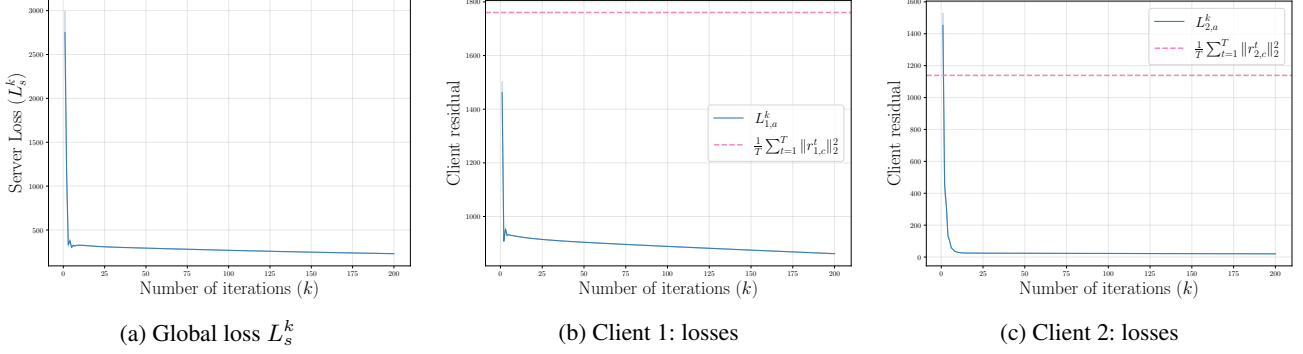


Figure 2: Global loss at the server and losses at the client from different models (augmented client loss: $L_{m,a}^k$, proprietary client loss: $\frac{1}{T} \sum_{t=1}^T \|r_{m,c}^t\|^2$) are plotted against the number of iterations (k).

Assumption 8.1 (Exogenous Input). The input u^t is zero-mean, *stationary*, *ergodic*, and independent of noises w^t , and v^t (Eq (1)), with $\mathbb{E}\|u^t\|^2 < \infty$. Moreover, u^t is *persistently excited* of order L if there exist $L \in \mathbb{N}$ and $\alpha > 0$ such that

$$\frac{1}{L} \sum_{k=t}^{t+L-1} u^k u^{k\top} \succeq \alpha I_{d_u} \quad \text{for all } t. \quad (23)$$

Lemma 8.2 (Normal equations). Under Assumption 8.1, at stationary points we have,

$$\begin{aligned} \mathbb{E}[(C_{mm}A_{mm})^\top r_{m,a}^{*,t} (y_m^{t-1})^\top] &= 0, \\ \mathbb{E}[C_{mm}^\top r_{m,a}^{*,t}] &= 0. \end{aligned} \quad (24)$$

where, $r_{m,a}^{*,t} = y_m^t - \tilde{y}_{m,a}^t(\theta_m^*, \phi_m^*)$, same as Eq. (6).

Theorem 8.3 (Convergence to the oracle). Assume $C_{mm}A_{mm}$ is full column rank and Assumption 8.1 holds. Then in the regime $\xi_m \rightarrow \infty$ we have,

$$\mathbb{E}[\tilde{y}_{m,o}^t - \tilde{y}_{m,a}^t(\theta_m^*, \phi_m^*)] = J_m \mathbb{E}[z_m^{t-1}]. \quad (25)$$

where, $z_m^{t-1} := [y_m^{t-1}; u^{t-1}; \hat{h}_{m,c}^{t-1}]$, $\Sigma_z := \mathbb{E}[z_m^{t-1} z_m^{t-1\top}]$, $e_t := C_{mm}(A_{mm}\theta_m^* y_m^{t-1} - \sum_{n \neq m} \hat{A}_{mn}^* \hat{h}_{n,c}^{t-1} + \phi_m^* - \sum_{n \neq m} \hat{B}_{mn}^* u_n^{t-1})$, and $J_m := \mathbb{E}[e_t z_m^{t-1\top}] \Sigma_z^{-1}$.

Lemma 8.2 states that, at stationarity, the augmented client residual is orthogonal (in expectation) to the local regressors it uses ($y_m^t, u^t, \hat{h}_{m,c}^t$); i.e., no further linear correction along those directions can reduce the residual. Theorem 8.3 then says that, when the client models have causal disentanglement ($\xi_m \rightarrow \infty$ regime), the federated reconstruction matches the oracle in expectation up to a bias $J_m \mathbb{E}[z_m^{t-1}]$.

9 EXPERIMENTS

9.1 SYNTHETIC DATASETS

We establish the performance of our algorithm on a multi-client LTI system described in Section 4.1. Unless otherwise

specified, we focus our experiments on a two-client system with $P_m = 2$, $U_m = 2$, and $D_m = 2$ for $m = \{1, 2\}$. A one-way directed dependency with $A_{12} = 0$ and $A_{21} \neq 0$ is considered for the ease of interpretation. The elements of input vectors are i.i.d. samples from a normal distribution $\mathcal{N}(0, 1)$. Clients use (4) and (5) to compute augmented state predictions and estimates. The proprietary client state estimate $\hat{h}_{m,c}^t$ is estimated in our experiment using a Kalman filter that uses only the client-specific (local) diagonal blocks (A_{mm}, B_{mm}, C_{mm}). The communication and training proceed as detailed in Section 5. The server maintains its state estimate according to (11), computed using current estimates of $\{\hat{A}_{mn}\}_{n \neq m}$ and $\{\hat{B}_{mn}\}_{n \neq m}$.

Training. Training curves are obtained after running 10 Monte-Carlo simulations. Each element of initial values of $\phi_m^0, \theta_m^0, \{\hat{A}_{mn}^0\}_{n \neq m}$ and $\{\hat{B}_{mn}^0\}_{n \neq m}$ for all $m = 1, 2, \dots, M$ are independently sampled from normal distributions. Global loss and client loss for both clients during training are plotted in Fig. 2a-2c. The baseline used for comparison is the time-averaged norm of residuals of the proprietary client model ($r_{m,c}^t := y_m^t - C_{mm} \hat{h}_{m,c}^t$). As training progresses, the augmented client loss $L_{m,a}$ outperforms the proprietary client loss. Thus, the parameters θ_m and ϕ_m , through the augmented client, encode cross-client interdependencies from off-diagonal blocks of A and B - which is not captured by the proprietary client model, validating Claim 5.3.

Validation. The estimated system is validated by plotting the prediction error on a new set of data generated from the same system (Figure 4). Both our models at the client (ACM) and the server performs better than the proprietary client model on the new data. Validation data contains a mean shift and is non-stationary, which causes a sudden jump in the performance of the model. Performance deterioration in our models due to mean shift is less than the proprietary model and the recovery is better.

Transfer Function. Following Section 6.1, the poles, zeros, and singular value spectra of the true and estimated transfer

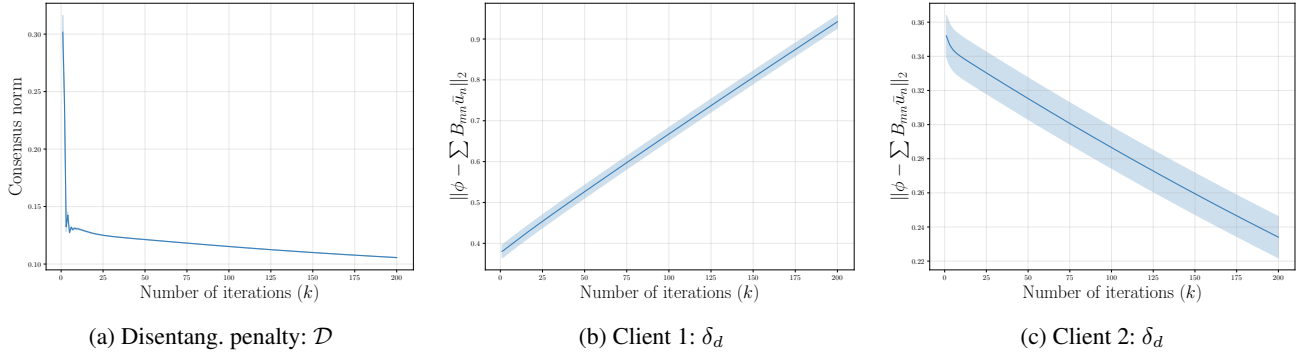


Figure 3: Disentanglement penalty at the server and δ_d at the clients vs. number of iterations.

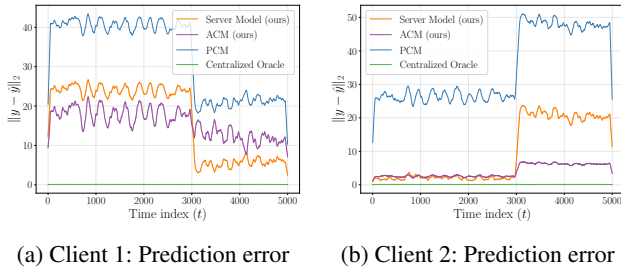


Figure 4: Prediction error on the validation data for different models and the centralized oracle. ACM: Augmented Client Model, PCM: Proprietary Client Model

functions Ljung [1998] are shown in Fig. 6. The estimated poles lie within the unit circle, confirming that the decentralized model preserves the stable dynamic structure of the ground truth. While some dispersion in the zeros and deviations in low-frequency singular values remain, the overall frequency-response profile is retained. Combined with the prediction performance in Fig. 4, these results indicate that our framework is approximating the underlying causal dynamics, while not yet fully recovering the centralized oracle, as expected under decentralized constraints.

Disentanglement. The disentanglement penalty \mathcal{D} at the server is plotted in Fig. 3a, and the difference $\delta_d := \|\phi_m - \frac{1}{T} \sum_{t=1}^T \left(\sum_{n \neq m} \hat{B}_{mn} u_n^{t-1} \right)\|_2$ is plotted for both clients in Fig. 3b and 3c. This demonstrates that not only server effectively disentangle the effect of inputs from the states, but it is also propagated to the respective clients. It was observed that there exists a trade-off between optimality and stability when employing the penalty \mathcal{D} . Details are provided in the Appendix 13.1.

Scalability. (i) We fix the number of clients M , state dimension P_m for each client and vary the measurement dimension D_m . (ii) The state dimension P_m and measurement dimension D_m for each client are fixed, and the number of clients is varied. Results of the scalability experiments can be found in the Appendix 13.1.

9.2 REAL-WORLD DATASETS

Experimental Setting. We evaluate our approach using two industrial cybersecurity datasets. The **HAI** dataset is generated using an industrial control system testbed integrated with a Hardware-in-the-Loop (HIL) simulator that models steam-turbine power generation and pumped-storage hydropower. The system includes four processes: (P1) Boiler, (P2) Turbine, (P3) Water Treatment, and (P4) HIL Simulation, each serving as a client in our experiments. The **SWaT** dataset originates from a six-stage water treatment plant testbed. Each stage is treated as a client in our experiments. We apply the following preprocessing steps to HAI/SWaT:

- **HAI.** All sensor measurements are first normalized to ensure consistent scaling. A subspace identification method is then applied to fit an LTI system, yielding a state-transition matrix A , input matrix B , and an observation matrix C . The dimensionality of the state space P_m is determined using the singular value decay of the Hankel matrix. Since the initial C is not block diagonal, we perform L_2 -norm based thresholding to assign each state variable to a specific process and construct a block diagonal C . Then, A and B are re-estimated via least squares.
- **SWaT.** For each client, only those variables with a Pearson correlation greater than 0.3 with other clients are retained. Then, the same subspace identification and re-estimation steps as in the HAI case are performed.

Results. Due to space constraints, we provide results for both real-world datasets in the Appendix 13.2.

10 LIMITATIONS

We assume LTI models, which may not capture real-world scenarios such as nonlinear or time-varying dynamics. Similarly, reliance on accurate proprietary client models and known local matrices may be unrealistic in practice. Clients can only infer the aggregated effects of counterfactual input. Convergence results only hold up to a bias in reconstruction.

References

- Martin Arjovsky, Léon Bottou, Ishaan Gulrajani, and David Lopez-Paz. Invariant risk minimization. *arXiv preprint arXiv:1907.02893*, 2019.
- Uri M. Ascher, Steven J. Ruuth, and Brian T. R. Wetton. Implicit-explicit methods for time-dependent partial differential equations. *SIAM Journal on Numerical Analysis*, 32(3):797–823, 1995. doi: 10.1137/0732037. URL <https://doi.org/10.1137/0732037>.
- Lionel Barnett, Adam B Barrett, and Anil K Seth. Granger causality and transfer entropy are equivalent for gaussian variables. *Physical Review Letters*, 103(23):238701, 2009.
- D.P. Bertsekas and W. Rheinboldt. *Constrained Optimization and Lagrange Multiplier Methods*. Computer science and applied mathematics. Academic Press, 2014. ISBN 9781483260471. URL <https://books.google.com/books?id=j6LiBQAAQBAJ>.
- Johann Brehmer, Pim De Haan, Phillip Lippe, and Taco S Cohen. Weakly supervised causal representation learning. *Advances in Neural Information Processing Systems*, 35:38319–38331, 2022.
- Michael Eichler. Granger causality and path diagrams for multivariate time series. *Statistical Modelling*, 10(3):233–255, 2010.
- Marco Fraccaro, Simon Kamronn, Ulrich Paquet, and Ole Winther. A disentangled recognition and nonlinear dynamics model for unsupervised learning. *Advances in neural information processing systems*, 30, 2017.
- John Geweke. Measurement of linear dependence and feedback between multiple time series. *Journal of the American Statistical Association*, 77(378):304–313, 1982.
- Shiuli Subhra Ghosh, Anmol Dwivedi, Ali Tajer, Kyongmin Yeo, and Wesley M. Gifford. Cascading failure prediction via causal inference. *IEEE Transactions on Power Systems*, 40(4):3361–3373, 2025. doi: 10.1109/TPWRS.2024.3516477.
- Clive WJ Granger. Investigating causal relations by econometric models and cross-spectral methods. *Econometrica*, 37(3):424–438, 1969.
- Xianjie Guo, Kui Yu, Lin Liu, and Jiuyong Li. Fedcsl: A scalable and accurate approach to federated causal structure learning. *Proceedings of the AAAI Conference on Artificial Intelligence*, 38(11):12235–12243, Mar. 2024.
- Biwei Huang, Kun Zhang, Mingming Gong, and Clark Glymour. Causal discovery and forecasting in nonstationary environments with state-space models. In *International conference on machine learning*, pages 2901–2910. Pmlr, 2019.
- Rudolph Emil Kalman. A new approach to linear filtering and prediction problems. *Transactions of the ASME—Journal of Basic Engineering*, 82(Series D):35–45, 1960.
- Rahul G Krishnan, Uri Shalit, and David Sontag. Deep kalman filters. *arXiv preprint arXiv:1511.05121*, 2015.
- Adam Li, Yushu Pan, and Elias Bareinboim. Disentangled representation learning in non-markovian causal systems. *Advances in Neural Information Processing Systems*, 37:104843–104903, 2024a.
- Loka Li, Ignavier Ng, Gongxu Luo, Biwei Huang, Guangyi Chen, Tongliang Liu, Bin Gu, and Kun Zhang. Federated causal discovery from heterogeneous data. *arXiv preprint arXiv:2402.13241*, 2024b.
- Phillip Lippe, Sara Magliacane, Sindy Löwe, Yuki M Asano, Taco Cohen, and Stratis Gavves. Citris: Causal identifiability from temporal intervened sequences. In *International Conference on Machine Learning*, pages 13557–13603. PMLR, 2022.
- L. Ljung. *System Identification: Theory for the User*. Pearson Education, 1998. ISBN 9780132440530. URL <https://books.google.com/books?id=fYSrk4wDKPsC>.
- Atalanti Mastakouri, David Rohde, and Bernhard Schölkopf. Necessary and sufficient conditions for causal feature selection in time series with latent confounders. In *NeurIPS*, 2021.
- Aditya P. Mathur and Nils Ole Tippenhauer. Swat: a water treatment testbed for research and training on ics security. In *2016 International Workshop on Cyber-physical Systems for Smart Water Networks (CySWater)*, pages 31–36, 2016. doi: 10.1109/CySWater.2016.7469060.
- Brendan McMahan, Eider Moore, Daniel Ramage, Seth Hampson, and Blaise y Arcas. Communication-efficient learning of deep networks from decentralized data. In *Artificial Intelligence and Statistics (AISTATS)*, 2017.
- Osman Mian, David Kaltenpoth, and Michael Kamp. Regret-based federated causal discovery. In Thuc Duy Le, Lin Liu, Emre Kıcıman, Sofia Triantafyllou, and Huan Liu, editors, *Proceedings of The KDD’22 Workshop on Causal Discovery*, volume 185 of *Proceedings of Machine Learning Research*, pages 61–69. PMLR, 15 Aug 2022.
- Osman Mian, David Kaltenpoth, Michael Kamp, and Jilles Vreeken. Nothing but regrets—privacy-preserving federated causal discovery. In *International Conference on Artificial Intelligence and Statistics*, pages 8263–8278. PMLR, 2023.
- Dorđe Miladinović, Muhammad Waleed Gondal, Bernhard Schölkopf, Joachim M Buhmann, and Stefan Bauer. Disentangled state space representations. *arXiv preprint arXiv:1906.03255*, 2019.

- Ayush Mohanty, Nazal Mohamed, Paritosh Ramanan, and Nagi Gebraeel. Federated granger causality learning for interdependent clients with state space representation. In *The Thirteenth International Conference on Learning Representations*, 2025.
- Kevin Patrick Murphy. *Dynamic Bayesian networks: representation, inference and learning*. PhD thesis, UC Berkeley, 2002.
- J. Pearl. *Causality*. Causality: Models, Reasoning, and Inference. Cambridge University Press, 2009. ISBN 9780521895606. URL <https://books.google.com/books?id=f4nuexsNVZIC>.
- Jonas Peters, Peter Bühlmann, and Nicolai Meinshausen. Causal inference by using invariant prediction: identification and confidence intervals. *Journal of the Royal Statistical Society Series B: Statistical Methodology*, 78(5):947–1012, 2016.
- Evangelos Pournaras, Riccardo Taormina, Manish Thapa, Stefano Galelli, Venkata Palleti, and Robert Kooij. Cascading failures in interconnected power-to-water networks. *SIGMETRICS Perform. Eval. Rev.*, 47(4):16–20, May 2020. ISSN 0163-5999. doi: 10.1145/3397776.3397781. URL <https://doi.org/10.1145/3397776.3397781>.
- Andres Ruiz-Tagle, Enrique Lopez-Droguett, and Katrina M. Groth. A novel probabilistic approach to counterfactual reasoning in system safety. *Reliability Engineering & System Safety*, 228:108785, 2022. ISSN 0951-8320.
- Bernhard Schölkopf, Francesco Locatello, Stefan Bauer, Nan Rosemary Ke, Nal Kalchbrenner, Anirudh Goyal, and Yoshua Bengio. Toward causal representation learning. *Proceedings of the IEEE*, 109(5):612–634, 2021.
- Hyeok-Ki Shin, Woomyo Lee, Jeong-Han Yun, and Byung-Gi Min. Two ics security datasets and anomaly detection contest on the hil-based augmented ics testbed. In *Cyber Security Experimentation and Test Workshop, CSET '21*, page 36–40, New York, NY, USA, 2021. Association for Computing Machinery. ISBN 9781450390651. doi: 10.1145/3474718.3474719. URL <https://doi.org/10.1145/3474718.3474719>.
- Wenbing Tang, Jing Liu, Yuan Zhou, and Zuohua Ding. Causality-guided counterfactual debiasing for anomaly detection of cyber-physical systems. *IEEE Transactions on Industrial Informatics*, 20(3):4582–4593, 2023.
- William Todo, Merwann Selmani, Béatrice Laurent, and Jean-Michel Loubes. Counterfactual explanation for multivariate times series using a contrastive variational autoencoder. In *ICASSP 2023-2023 IEEE International Conference on Acoustics, Speech and Signal Processing (ICASSP)*, pages 1–5. IEEE, 2023.
- Xin Wang, Hong Chen, Si'ao Tang, Zihao Wu, and Wenwu Zhu. Disentangled representation learning. *IEEE Transactions on Pattern Analysis and Machine Intelligence*, 46(12):9677–9696, 2024.
- Zixuan Weng, Jindong Han, Wenzhao Jiang, and Hao Liu. Sde: A simplified and disentangled dependency encoding framework for state space models in time series forecasting. In *Proceedings of the 31st ACM SIGKDD Conference on Knowledge Discovery and Data Mining V. 2*, pages 3168–3179, 2025.
- Dezhi Yang, Xintong He, Jun Wang, Guoxian Yu, Carlotta Domeniconi, and Jinglin Zhang. Federated causality learning with explainable adaptive optimization. *Proceedings of the AAAI Conference on Artificial Intelligence*, 38(15):16308–16315, Mar. 2024.
- Qiaoling Ye, Arash A. Amini, and Qing Zhou. Federated learning of generalized linear causal networks. *IEEE Transactions on Pattern Analysis and Machine Intelligence*, 46(10):6623–6636, 2024.
- Yongsheng Zhao, Kui Yu, Guodu Xiang, Xianjie Guo, and Fuyuan Cao. Fedece: Federated estimation of causal effect based on causal graphical modeling. *IEEE Transactions on Artificial Intelligence*, 6(8):2327–2341, 2025.

Federated Causal Representation Learning in State-Space Systems for Decentralized Counterfactual Reasoning (Supplementary Material)

11 Privacy Analysis	12
11.1 Notation and Sensitivity	12
11.2 Noise Mechanisms and Calibration	12
11.3 Composition and Post-Processing	13
12 Gradients Communicated by the Server	14
13 Experiments	16
13.1 Additional Results on Synthetic Datasets	16
13.2 Real-world Datasets	17
14 Pseudocode	21
15 Proofs	22
15.1 Derivatives of L_s with respect to client parameters θ_m and ϕ_m	22
15.2 Proposition 4.1	23
15.3 Theorem 6.1	24
15.4 Corollary 6.2	24
15.5 Lemma 7.2	25
15.6 Theorem 7.3	25
15.7 Lemma A.6	27
15.8 Lemma A.8	27
15.9 Proposition A.11	27
15.10 Proposition A.12	28
15.11 Corollary A.13	28

11 PRIVACY ANALYSIS

11.1 NOTATION AND SENSITIVITY

Definition 11.1 (Local dataset and horizon). For each client m , the private dataset is $\mathcal{D}_m = \{y_m^t\}_{t=1}^T$, collected over a fixed horizon $T \in \mathbb{N}$. The union $\mathcal{D} = \{\mathcal{D}_1, \dots, \mathcal{D}_M\}$ denotes all clients' measurement data.

Definition 11.2 (Neighboring datasets). Two global datasets \mathcal{D} and \mathcal{D}' are *neighbors* if they differ at a single measurement $y_{m^*}^{t^*}$ for some client m^* and time t^* .

Assumption 11.3 (Bounded and clipped signals). Input u_m^t and output (or measurements) y_m^t are bounded (to ensure stability of state-spaces), and are clipped to those known bounds: $\|y_m^t\|_2 \leq R_y$, and $\|u_m^t\|_2 \leq R_u$. The maximum magnitude across all input/output signals is denoted by $R_{\max} = \max(R_y, R_u)$.

Rationale: Clipping in Assumption 11.3 ensures bounded sensitivity prior to noise addition.

Assumption 11.4 (Local estimator contractivity). Each client's augmented estimator is contractive with constants $L_m > 0$ and $\beta_m \in (0, 1)$: $\|h_{m,a}^t - h_{m,a}^{t'}\|_2 \leq L_m \beta_m^{t-s} \|y_m^s - y_m^{s'}\|_2$, $\forall s \leq t$.

Rationale: Assumption 11.4 ensures bounded propagation of perturbations in local measurements.

Let $z_m^t = [\hat{h}_{m,c}^t; \hat{h}_{m,a}^t; h_{m,a}^t; u_m^t] \in \mathbb{R}^{3P_m + U_m}$ be the message communicated from client m to the server.

Definition 11.5 (Message generation map). The deterministic, pre-noise mapping from measurements to the transmitted message is given as $\mathcal{M}_{m,\text{msg}}^t : (y_m^{1:t}) \mapsto z_m^t$. This map depends on the internal dynamics of the proprietary and augmented estimators.

Lemma 11.6 (ℓ_2 -Sensitivity of client messages). Under bounded measurements and contractive estimators, there exists $\kappa_m > 0$ such that for any neighboring datasets \mathcal{D}_m and \mathcal{D}'_m differing at one $y_m^{t^*}$,

$$\|\mathcal{M}_{m,\text{msg}}^t(\mathcal{D}_m) - \mathcal{M}_{m,\text{msg}}^t(\mathcal{D}'_m)\|_2 \leq \Delta_{m,\text{msg}} = \kappa_m R_{\max}.$$

Remark 11.7 (Role of block-diagonal C). In our paper, the observation matrix C is block-diagonal. When C is block-diagonal (so that $y_m^t = C_{mm} h_m^t$), each client's κ_m depends only on its own local block.

The server communicates the gradient $g_m^t := \nabla_{h_{m,a}^t} L_s$ to client m . Given the expression of server loss L_s in Eq (13), the analytical expression of g_m can be computed as,

$$g_m^t = \frac{2}{T} \left(h_{m,a}^t - [A_{mm} \hat{h}_{m,c}^{t-1} + \sum_{n \neq m} \hat{A}_{mn} \hat{h}_{n,c}^{t-1} + B_{mm} u_m^{t-1} + \sum_{n \neq m} \hat{B}_{mn} u_n^{t-1}] \right),$$

Lemma 11.8 (ℓ_2 -Sensitivity of server gradients). Given the expression of g_m^t above, the sensitivity with respect to one changed measurement $y_{m'}^{t^*}$ (for some client m' and time t^*) is bounded by

$$\|g_m^t - g_m^{t'}\|_2 \leq \Delta_{m,\text{grad}} = \frac{2}{T} (1 + \|A_{mm}\|) \kappa_{m,\text{mix}} R_{\max},$$

where the constant $\kappa_{m,\text{mix}}$ is given explicitly as

$$\kappa_{m,\text{mix}} = L_{m'} \left(\|C_{mm}\| + \sum_{n \neq m} (\|A_{mn}\| \beta_n^{t-t^*} + \|B_{mn}\|) \right).$$

where, $L_{m'}$ arises from the local contractivity bound in Assumption 11.4.

11.2 NOISE MECHANISMS AND CALIBRATION

Definition 11.9 (Clipping constants). Each client enforces ℓ_2 -norm clipping thresholds $C_{\text{msg}}, C_{\text{grad}} > 0$, so that $\|z_m^t\|_2 \leq C_{\text{msg}}$ and $\|g_m^t\|_2 \leq C_{\text{grad}}$ for all m, t . These are chosen such that

$$C_{\text{msg}} \geq \Delta_{m,\text{msg}}, \quad C_{\text{grad}} \geq \Delta_{m,\text{grad}}.$$

where $\Delta_{m,\text{msg}}$ and $\Delta_{m,\text{grad}}$ denote the ℓ_2 -sensitivities of the client message and server gradients, respectively.

Definition 11.10 (Perturbation). Privacy is achieved by adding independent Gaussian noise:

$$\tilde{z}_m^t = z_m^t + \mathcal{N}(0, \sigma_{\text{msg}}^2 C_{\text{msg}}^2 I), \quad \tilde{g}_m^t = g_m^t + \mathcal{N}(0, \sigma_{\text{grad}}^2 C_{\text{grad}}^2 I).$$

Noise multipliers σ_{msg} and σ_{grad} are selected to achieve target privacy parameters (ε, δ) .

Proposition 11.11 (Per-release Gaussian DP). For the client m 's message and server gradient release mechanisms, the sufficient noise multipliers satisfying (ε, δ) -DP are

$$\sigma_{\text{msg}} \geq \frac{\Delta_{m,\text{msg}}}{C_{\text{msg}}} \sqrt{2 \ln \left(\frac{1.25}{\delta} \right)} \frac{1}{\varepsilon_{\text{msg}}}, \quad \sigma_{\text{grad}} \geq \frac{\Delta_{m,\text{grad}}}{C_{\text{grad}}} \sqrt{2 \ln \left(\frac{1.25}{\delta} \right)} \frac{1}{\varepsilon_{\text{grad}}}.$$

The Gaussian perturbation scales σ_{msg} and σ_{grad} quantify privacy strength for the message and gradient channels. Larger noise yields stronger privacy at the expense of higher variance in estimated parameters. Clipping thresholds C_{msg} and C_{grad} cap the maximum influence of any single measurement y_m^t , ensuring the injected noise dominates any one individual's contribution.

11.3 COMPOSITION AND POST-PROCESSING

Proposition 11.12 (Sequential and joint composition of Gaussian mechanisms). Let each client m release privatized messages \tilde{z}_m^t and gradients \tilde{g}_m^t over R communication rounds. If each mechanism satisfies $(\varepsilon_{\text{msg}}, \delta_{\text{msg}})$ -DP for messages and $(\varepsilon_{\text{grad}}, \delta_{\text{grad}})$ -DP for gradients, then the composition across all rounds satisfies,

$$(\varepsilon_{\text{total}}, \delta_{\text{total}}) = (R(\varepsilon_{\text{msg}} + \varepsilon_{\text{grad}}), R(\delta_{\text{msg}} + \delta_{\text{grad}})).$$

Corollary 11.13 (Post-processing invariance). All downstream quantities, including the server's learned matrices $\{\hat{A}_{mn}, \hat{B}_{mn}\}$, client parameters $\{\theta_m, \phi_m\}$, and counterfactual outputs, retain the same (ε, δ) privacy guarantee as the privatized training transcript.

12 GRADIENTS COMMUNICATED BY THE SERVER

Proposition 12.1. *Using the chain rule, the derivatives of the server loss L_s with respect to the augmented client parameters of client m (i.e., ϕ_m and θ_m) are*

$$\begin{aligned}\nabla_{\theta_m} L_s &= \sum_{t=1}^T (A_{mm}^\top \nabla_{h_{m,a}^t} L_s + \nabla_{\hat{h}_{m,a}^{t-1}} L_s) y_m^{t-1\top}, \text{ and} \\ \nabla_{\phi_m} L_s &= \sum_{t=1}^T \nabla_{h_{m,a}^t} L_s.\end{aligned}$$

Proof. From the augmented client model,

$$h_{m,a}^t = A_{mm} \hat{h}_{m,a}^{t-1} + b_m^{t-1} + \phi_m, \quad \hat{h}_{m,a}^{t-1} = c_m^{t-1} + \theta_m y_m^{t-1}.$$

Consider the proxy loss,

$$\ell(h_{m,a}^t, \hat{h}_{m,a}^{t-1}) := \frac{1}{T} \sum_{t=1}^T \left(\|h_{m,a}^t - X_m^t\|_2^2 + \xi \|A_{mm} \hat{h}_{m,a}^{t-1} - Z_m^{t-1}\|_2^2 \right),$$

This proxy loss follows the same computational graph as the client model with,

$$h^t = A_{mm} \hat{h}^{t-1} + b^{t-1} + \phi, \quad \hat{h}^{t-1} = c^{t-1} + \theta y^{t-1}.$$

Using **Einstein index notation**, repeated Latin indices are summed over automatically. Indices $p, k, r \in \{1, \dots, P_m\}$ denote state components and $j, s \in \{1, \dots, D_m\}$ denote measurement components. The Kronecker delta is δ_{ij} , and subscripts on a vector or matrix denote its components.

Derivative with respect to θ_m . By the chain rule,

$$\frac{\partial \ell}{\partial \theta_{m,rs}} = \frac{1}{T} \sum_{t=1}^T \sum_{p=1}^{P_m} \left(\frac{\partial \ell}{\partial h_{m,a,p}^t} \frac{\partial h_{m,a,p}^t}{\partial \theta_{m,rs}} + \frac{\partial \ell}{\partial \hat{h}_{m,a,p}^{t-1}} \frac{\partial \hat{h}_{m,a,p}^{t-1}}{\partial \theta_{m,rs}} \right).$$

From

$$h_{m,a,p}^t = A_{mm,pk} \hat{h}_{m,a,k}^{t-1} + b_{m,p}^{t-1} + \phi_{m,p}, \quad \hat{h}_{m,a,k}^{t-1} = c_{m,k}^{t-1} + \theta_{m,kj} y_{m,j}^{t-1},$$

we have

$$\frac{\partial \hat{h}_{m,a,k}^{t-1}}{\partial \theta_{m,rs}} = \delta_{kr} y_{m,s}^{t-1}, \quad \frac{\partial h_{m,a,p}^t}{\partial \theta_{m,rs}} = A_{mm,pk} \frac{\partial \hat{h}_{m,a,k}^{t-1}}{\partial \theta_{m,rs}} = A_{mm,pk} \delta_{kr} y_{m,s}^{t-1} = A_{mm,pr} y_{m,s}^{t-1}.$$

Hence,

$$\begin{aligned}\frac{\partial \ell}{\partial \theta_{m,rs}} &= \frac{1}{T} \sum_{t=1}^T \left[\left(\frac{\partial \ell}{\partial h_{m,a,p}^t} \right) A_{mm,pr} + \left(\frac{\partial \ell}{\partial \hat{h}_{m,a,p}^{t-1}} \right) \delta_{pr} \right] y_{m,s}^{t-1} \\ &= \frac{1}{T} \sum_{t=1}^T \left[(A_{mm}^\top \nabla_{h_{m,a}^t} \ell)_r + (\nabla_{\hat{h}_{m,a}^{t-1}} \ell)_r \right] y_{m,s}^{t-1}.\end{aligned}$$

Collecting the (r, s) -entries, the matrix form is

$$\nabla_{\theta_m} \ell = \frac{1}{T} \sum_{t=1}^T (A_{mm}^\top \nabla_{h_{m,a}^t} \ell + \nabla_{\hat{h}_{m,a}^{t-1}} \ell) (y_m^{t-1})^\top.$$

Derivative with respect to ϕ_m . Again by the chain rule,

$$\frac{\partial \ell}{\partial \phi_{m,a}} = \frac{1}{T} \sum_{t=1}^T \sum_{p=1}^{P_m} \frac{\partial \ell}{\partial h_{m,a,p}^t} \frac{\partial h_{m,a,p}^t}{\partial \phi_{m,a}} = \frac{1}{T} \sum_{t=1}^T \sum_{p=1}^{P_m} \frac{\partial \ell}{\partial h_{m,a,p}^t} \delta_{pa} = \frac{1}{T} \sum_{t=1}^T [\nabla_{h_{m,a}^t} \ell]_a,$$

or in matrix form,

$$\nabla_{\phi_m} \ell = \frac{1}{T} \sum_{t=1}^T \nabla_{h_{m,a}^t} \ell.$$

Finally, replacing ℓ by L_s (the factor $1/T$ is an inconsequential constant) yields

$$\nabla_{\theta_m} L_s = \sum_{t=1}^T (A_{mm}^\top \nabla_{h_{m,a}^t} L_s + \nabla_{\hat{h}_{m,a}^{t-1}} L_s) y_m^{t-1\top}, \quad \nabla_{\phi_m} L_s = \sum_{t=1}^T \nabla_{h_{m,a}^t} L_s,$$

as claimed. □

13 EXPERIMENTS

13.1 ADDITIONAL RESULTS ON SYNTHETIC DATASETS

The results plotted in Fig. 3 are obtained by directly optimizing the server loss (Eq 13) with the disentanglement penalty ξ and tuning the learning rates. It was observed that direct implementation of the penalty-based disentanglement could make the framework unstable for large values ξ - which is a requirement for effective disentanglement. This issue can be mitigated by implementing an Augmented Lagrangian method (Bertsekas and Rheinboldt [2014]), which results in better disentanglement while keeping the framework stable. However, the Augmented Lagrangian method might converge sub-optimal solution compared to the penalty-based disentanglement. We explain this in the next paragraph.

Augmented Lagrangian with IMEX To robustify training under large penalty ξ and improve local disentanglement, we also experimented with an Augmented Lagrangian (AL) formulation Bertsekas and Rheinboldt [2014] combined with an implicit-explicit (IMEX) time discretization Ascher et al. [1995]. In AL (as opposed to the **Penalty Method (PM)** which optimizes L_s at the server), the hard alignment/consensus condition is enforced via a quadratic penalty and a dual term λ (similar to a Lagrangian multiplier), i.e., we update the server and client variables by minimizing the AL server loss,

$$\mathcal{L}_{\text{AL}} = \frac{1}{T} \sum_{t=1}^T \sum_{m=1}^M \left(\|r_{m,s}^t\|_2^2 + \lambda_m^{t\top} \mathcal{D}_m^t + \frac{\rho}{2} \|\mathcal{D}_m^t\|_2^2 \right),$$

where

$$\mathcal{D}_m^t := A_{mm}(\hat{h}_{m,a}^{t-1} - \hat{h}_{m,c}^{t-1}) - \sum_{n \neq m} \hat{A}_{mn} \hat{h}_{n,c}^{t-1}$$

and $\rho > 0$ is the penalty. Practically, this stabilizes training under large penalties and promotes cleaner separation of client-specific and cross-client effects (“disentanglement”). The trade-off is that the IMEX/AL step solves a proximal, constraint-regularized surrogate rather than the original unconstrained gradient step at each iteration; hence the fixed point can be slightly biased and, in that sense, suboptimal relative to our primary (non-AL) method, even though it is often better behaved numerically.

For all our experiments, other than for this part, we have implemented the Penalty Method. In Figure 5, we have compared the Penalty Method (PM) and Augmented Lagrangian (AL). The learning curve of AL exhibits larger oscillations but achieves better disentanglement quickly at both server and clients (Figures 5b, 5e and 5f). This suggests in practice we can use a hybrid schedule: use AL as a warm start to quickly enforce disentanglement, then switch to PM to achieve a smoother descent of L_s and a marginally better final objective.

Scalability: We study the scalability of our framework in two ways: **(i)** For a two component system, we fix the state dimension $P_m = 2$, input dimension $U_m = 2$ and generate stable LTI systems with measurement dimensions $D_m = \{16, 32, 64, 128\}$. We report the final server loss function L_s and the disentanglement norm \mathcal{D} in Table 1. **(ii)** The state, input and output dimensions are fixed at $P_m = 2, U_m = 2$ and $D_m = 8$ respectively. The number of clients are varied as $M = \{2, 4, 8, 16\}$. As before, the final server loss L_s and \mathcal{D} are reported in Table 2

Table 1: L_s and \mathcal{D} by scaling measurement dim. D_m

$D_m = 16$		$D_m = 32$		$D_m = 64$		$D_m = 128$	
L_s	\mathcal{D}	L_s	\mathcal{D}	L_s	\mathcal{D}	L_s	\mathcal{D}
0.7649	0.0034	1.0987	0.0041	1.4243	0.0046	1.1805	0.0047

Table 2: Server loss L_s by scaling number of clients M

$M = 2$		$M = 4$		$M = 8$		$M = 16$	
L_s	\mathcal{D}	L_s	\mathcal{D}	L_s	\mathcal{D}	L_s	\mathcal{D}
0.0744	0.0013	0.0412	0.0010	0.1714	0.0036	0.3825	0.0069

From Tables 1 and 2, it is clear that as the observation dimension D_m and the number of clients M increase, the performance degrades. Scaling D_m impacts the objective more: with P_m fixed, the model must explain an ever larger output space

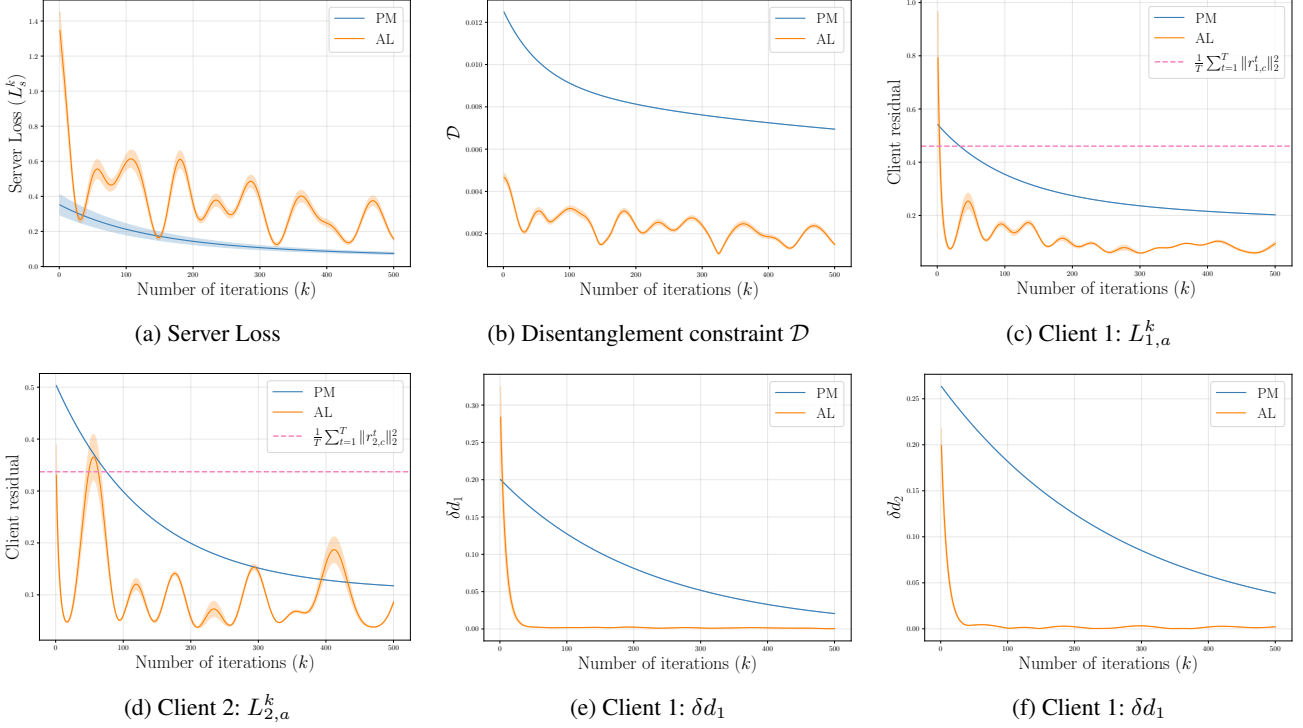


Figure 5: Comparison between Penalty Method (PM) and Augmented Lagrangian (AL) for the two client system. L_s , \mathcal{D} , Local loss (client residual) $L_{m,a}$ and δd_m vs Number of iterations (k) are plotted. Note that we defined $\delta d_m := \|\phi_m - \frac{1}{T} \sum_{t=1}^T (\sum_{n \neq m} \hat{B}_{mn} u_n^{t-1})\|_2$

with a low-dimensional latent state. This makes the observation map C increasingly tall, amplifies estimation variance and sensor noise aggregation, and exposes unmodeled sensor-specific dynamics; consequently L_s rises even though \mathcal{D} remains small. Increasing M introduces more inter-client couplings (off-diagonal A_{mn} , B_{mn} blocks) and consensus constraints to disentangle; the larger, more heterogeneous optimization also raises gradient variance and complicates stepsize selection, leading to a milder but noticeable growth in L_s and \mathcal{D} . Overall, the disentanglement metric remains low across all settings ($\mathcal{D} \leq 7 \times 10^{-3}$), indicating that the method preserves separation even as scale grows.

Transfer Function: Poles, zeros, and the spectrum of singular values for the transfer function of estimated and true system are given in Figure 6

13.2 REAL-WORLD DATASETS

HAI dataset (v21.03) Shin et al. [2021]: The HAI industrial control dataset logs a multi-unit process with four coupled subsystems (clients), which we refer to as **P1–P4**. Tags are prefixed by the process identifier (e.g., P1_, P2_, P3_, P4_). Within each process, *sensor* channels (e.g., level/flow/pressure/temperature transmitters) are continuous, while *actuator/command* channels (e.g., valve commands and pump toggles) are predominantly discrete. In our federated setting we map *client k* to *process P_k* simply by this prefix rule. Inputs U are taken from actuator/command tags for that process (e.g., FCV/LCV/PCV/PP/OnOff/AutoGO/RTR families), and outputs Y are the continuous transmitter tags (e.g., LIT/FIT/PIT/TIT/SIT/V*T* families), as specified in the HAI tag manual.

Preprocessing Starting from the vendor CSV logs, we (i) time-align and parse headers; (ii) remove *constant* channels over the full run and re-check after truncation; (iii) prune discrete-like signals before modeling (drop boolean-like and quasi-discrete channels with low transition counts or extreme dominance); (iv) split variables into U and Y by tag family and process prefix; (v) standardize each column by z -scoring and save the means/stds; and (vi) fit a centralized LTI model with unconstrained A , B while enforcing block-diagonal C , Q , R by process. The identified states are then partitioned to processes by maximizing energy of the corresponding C -columns on each process’ outputs, with a fix-up step to guarantee

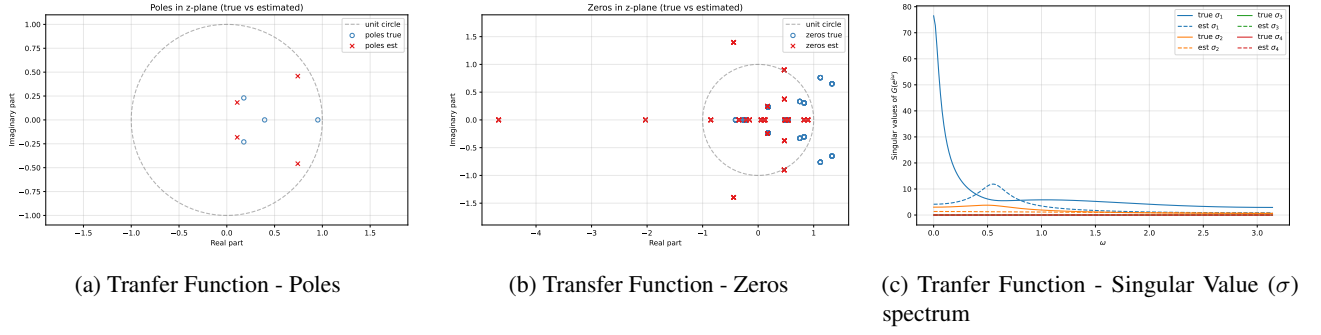


Figure 6: Transfer Function characteristics

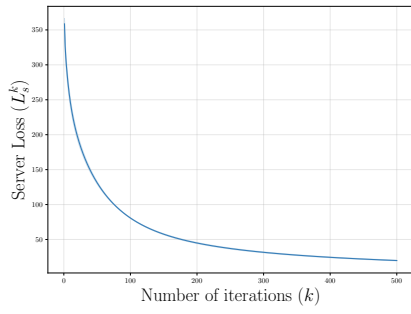
at least one state per active process.

Figure 7 shows a consistent convergence story across all panels. The server loss L_s^k (a) decays rapidly in the first few dozen iterations and then tapers off smoothly, indicating a stable approach to a low-loss regime without oscillations. The disentanglement constraint \mathcal{D} (b) follows the same pattern, decreasing monotonically and confirming that the consensus/coupling conditions are being enforced as optimization proceeds. Overall, the results show fast, stable convergence on HAI with uniformly small constraints and residuals at the end, despite mild per-client differences in the transient

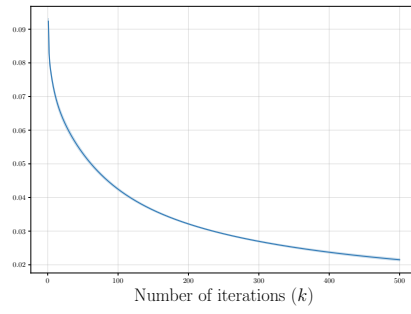
SWaT Dataset Mathur and Tippenhauer [2016] . The Secure Water Treatment (SWaT) plant is a six-stage potable water facility with tightly controlled pumping, filtration, and disinfection units. Tags follow the instrumentation manual convention: process equipment identifiers (e.g., MV101, P201, UV401) embed the stage in the leading digit. We map federated clients to stages S1–S6 using this digit. Manipulated variables (inputs) come from actuator and command tags—motorised valves (MV***), pumps (P***), UV toggles, and setpoint/command channels. Measurements (outputs) are the continuous transmitters: flow (FIT***), level (LIT***), differential pressure (DPIT***), pressure (PIT***), analogue analysers, etc. Unlike HAI, actuators are almost fully discrete, so we treat them as binary bits (after collapsing occasional tri-state encodings) and reserve all real-valued telemetry for outputs.

Preprocessing : (i) promote the first row to the header, relabel columns, and align timestamps; (ii) drop constant channels globally and again after truncating to the first 30000 samples; (iii) detect and remove quasi-discrete or boolean-like signals on the measurement side; (iv) classify each tag into inputs or outputs using stage-aware regex heuristics and split per stage; (v) z-score every column, saving the means/standard deviations; and (vi) add small Gaussian noise to the (otherwise discrete) input channels so the centralized LTI identification has non-degenerate excitation. We then identify a centralized LTI model with unconstrained (A , B) but enforce block-diagonal (C , Q , R) by stage. States are assigned to stages (clients) via the energy of their (C)-columns on each stage’s outputs, with a fix-up to ensure every active stage owns at least one state before exporting per-stage component folders.

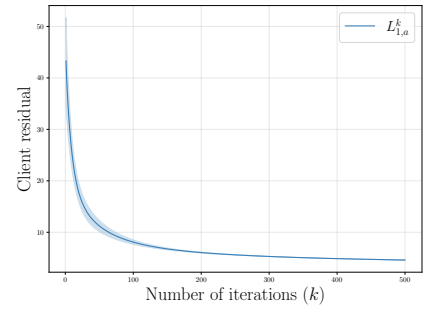
The results from SWaT dataset are plotted in Figure 8. Similar to the results from the HAI dataset, Figure 8 illustrates the convergence behavior observed on the SWaT dataset. The server loss L_s^k (a) exhibits a sharp initial decline followed by a smooth saturation phase, indicating a stable approach toward a low-loss regime with no noticeable oscillations. The disentanglement constraint \mathcal{D} (b) follows a similar monotonic decreasing trend, demonstrating that the consensus and coupling constraints are effectively enforced throughout optimization. Due to the large scale of the SWaT dataset and the constraints of available computational resources, Monte Carlo simulations were not performed; consequently, the reported results correspond to a single representative sample path.



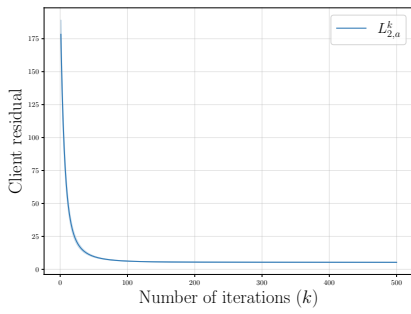
(a) Server Loss



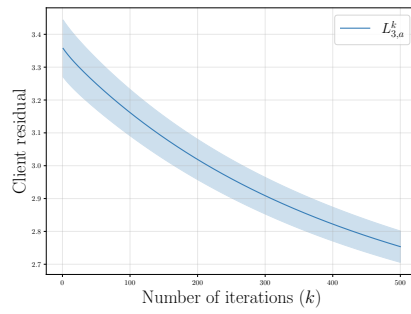
(b) \mathcal{D}



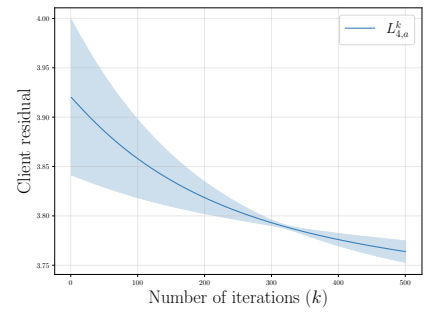
(c) Client 1: $L_{1,a}^k$



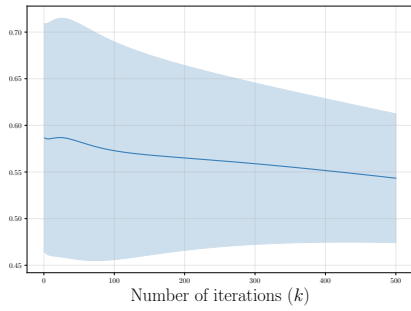
(d) Client 2: $L_{2,a}^k$



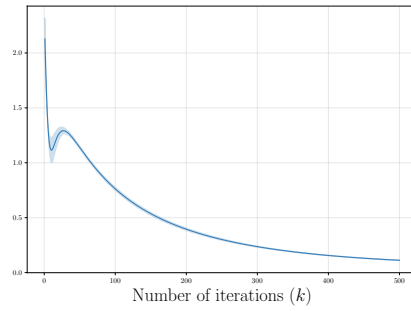
(e) Client 3: $L_{3,a}^k$



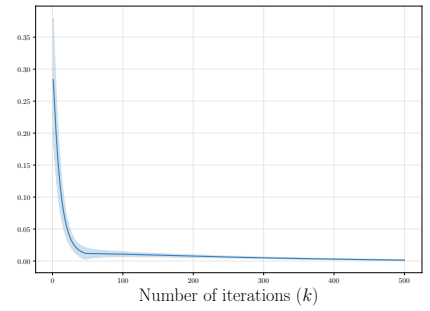
(f) Client 4: $L_{4,a}^k$



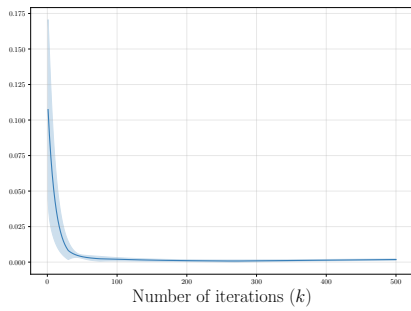
(g) Client 1: δd_1



(h) Client 2: δd_2

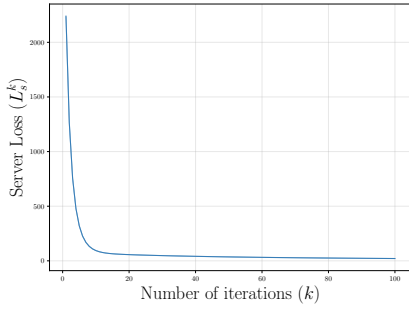


(i) Client 3: δd_3

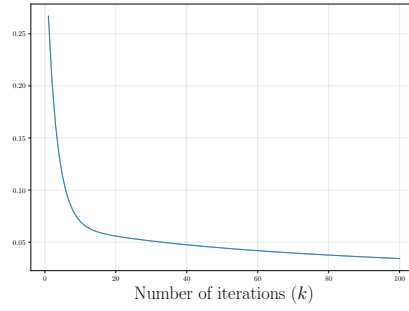


(j) Client 4: δd_4

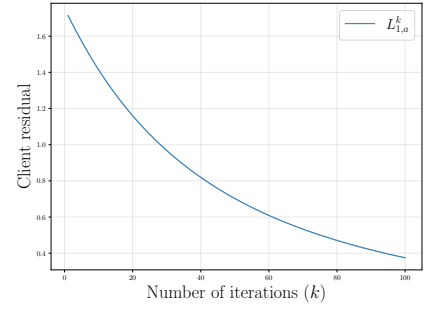
Figure 7: HAI dataset



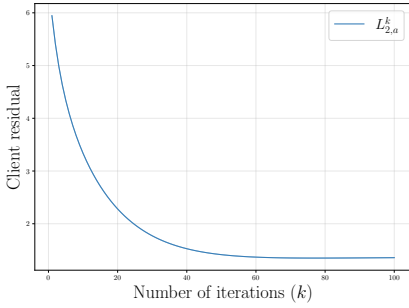
(a) Server Loss



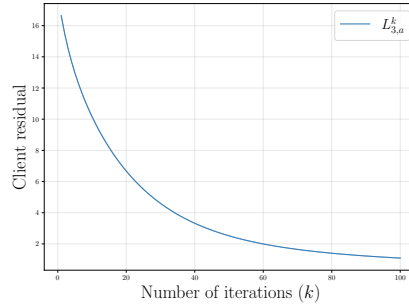
(b) \mathcal{D}



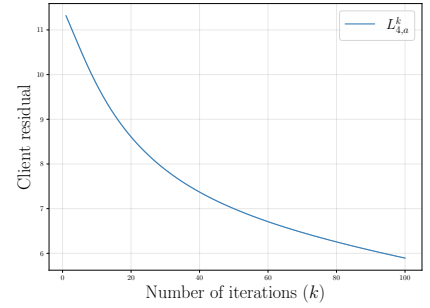
(c) Client 1: $L_{1,a}^k$



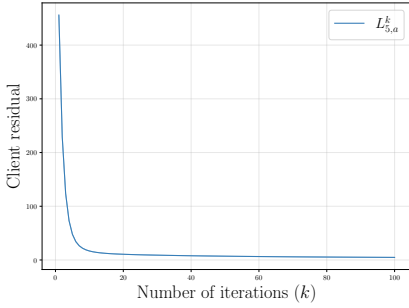
(d) Client 2: $L_{2,a}^k$



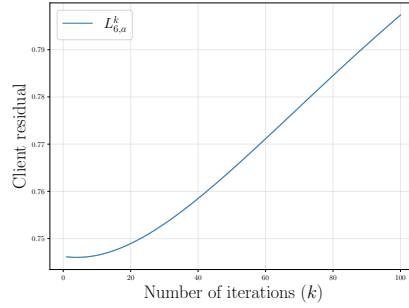
(e) Client 3: $L_{3,a}^k$



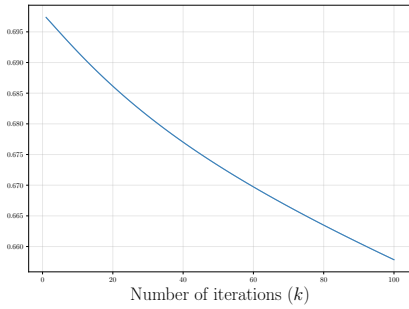
(f) Client 4: $L_{4,a}^k$



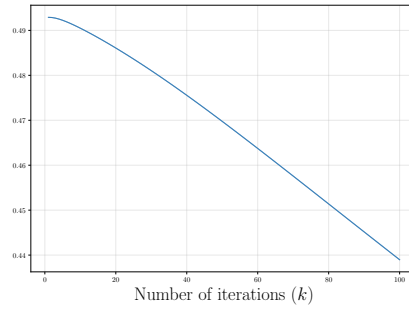
(g) Client 5: $L_{5,a}^k$



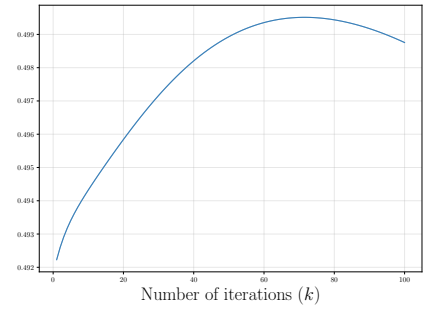
(h) Client 6: $L_{6,a}^k$



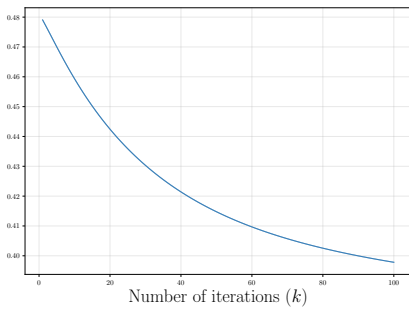
(i) Client 1: δd_1



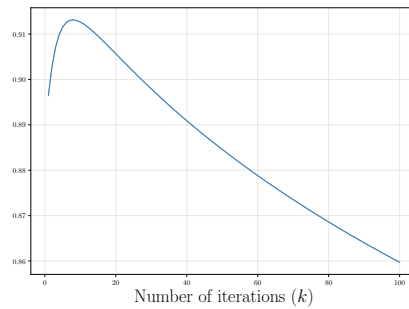
(j) Client 2: δd_2



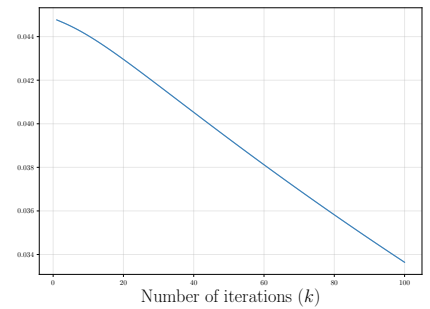
(k) Client 3: δd_3



(l) Client 4: δd_4



(m) Client 5: δd_5



(n) Client 6: δd_6

Figure 8: SWaT dataset

14 PSEUDOCODE

Refer to Algorithm 1 for the pseudocode of the proposed federated learning framework.

Algorithm 1 Federated Learning of \hat{A}_{mn} and \hat{B}_{mn}

```

1: Inputs:  $T, A_{mm}, B_{mm}, C_{mm}, \hat{h}_{m,c}^t, u_m^t \forall m \in \{1, \dots, M\}, t \in \{1, \dots, T\}$ 
2: Choose: iterations, tolerance  $tol$ , set  $k = 0$ 
3: Initialize at Server:  $\{\hat{A}_{mn}^0\}_{m \neq n}, \{\hat{B}_{mn}^0\}_{m \neq n}$ 
4: Choose at Server: learning rates  $\alpha_A, \alpha_B, \{\xi_m\} \forall m$ 
5: Initialize at Client  $m$ :  $\theta_m^0, \phi_m^0, \hat{h}_{m,a}^{0,t} \forall t$ 
6: Choose at Client:  $\eta_1, \eta_2, \gamma_1, \gamma_2$ 
7: while  $k < iterations$  or  $L_s > tol$  do
8:   for Each client  $m$  do
9:     for  $t = 1$  to  $T$  do
10:       $h_{m,a}^{k,t} \leftarrow A_{mm} \cdot \hat{h}_{m,a}^{k,t-1} + B_{mm} \cdot u_m^{t-1} + \phi_m^k$ 
11:       $r_{m,a}^{k,t} \leftarrow y_m^t - C_{mm} h_{m,a}^{k,t}$ 
12:       $\hat{h}_{m,a}^{k,t} \leftarrow \hat{h}_{m,c}^t + \theta_m^k y_m^t$ 
13:       $L_{m,a}^k \leftarrow L_{m,a}^k + \frac{1}{T} \|r_{m,a}^{k,t}\|_2^2$ 
14:     end for
15:     if  $k = 0$  then
16:       Send  $\left\{ h_{m,a}^{k,t}, \hat{h}_{m,a}^{k,t-1}, \hat{h}_{m,c}^{t-1}, u_m^{t-1} \right\}_{t=1}^T$  to the server
17:     else
18:       Send  $\left\{ h_{m,a}^{k,t} \right\}_{t=1}^T$  to the server
19:     end if
20:   end for
21:   for [At the Server] do
22:     for  $t = 1$  to  $T$  do
23:       for each  $m$  do
24:          $h_{m,s}^{k,t} \leftarrow A_{mm} \cdot \hat{h}_{m,c}^{t-1} + B_{mm} u_m^{t-1} + \sum_{n \neq m} (\hat{A}_{mn}^k \cdot \hat{h}_{n,c}^{t-1} + \hat{B}_{mn}^k \cdot u_n^{t-1})$ 
25:       end for
26:        $g_s^{k,t} := \sum_{m=1}^M \left( \|h_{m,a}^{k,t} - h_{m,s}^{k,t}\|_2^2 + \xi \|A_{mm}(\hat{h}_{m,a}^{k,t-1} - \hat{h}_{m,c}^{t-1}) - \sum_{n \neq m} \hat{A}_{mn} \hat{h}_{n,c}^{t-1}\|_2^2 \right)$ 
27:        $\nabla_{h_{m,a}^{k,t}} L_s \leftarrow \frac{1}{T} \nabla_{h_{m,a}^{k,t}} g_s^{k,t}$ 
28:        $L_s^k \leftarrow L_s^k + \frac{1}{T} g_s^{k,t}$ 
29:     end for
30:      $\hat{A}_{mn}^{k+1} \leftarrow \hat{A}_{mn}^k - \alpha_A \cdot \nabla_{\hat{A}_{mn}^k} L_s^k$ 
31:      $\hat{B}_{mn}^{k+1} \leftarrow \hat{B}_{mn}^k - \alpha_B \cdot \nabla_{\hat{B}_{mn}^k} L_s^k$ 
32:     Send  $\left\{ \nabla_{h_{m,a}^{k,t}} L_s^k \right\}_{t=1}^T$  to client  $m$ 
33:   end for
34:   for Each client  $m$  do
35:     for  $t = 1$  to  $T$  do
36:        $\nabla_{\theta_m^k} L_s^k \leftarrow \nabla_{\theta_m^k} L_s^k + A_{mm}^\top \left( \nabla_{h_{m,a}^t} L_s^k \right) y_m^{t-1 \top}$ 
37:     end for
38:      $\theta_m^{k+1} \leftarrow \theta_m^k - \eta_1 \cdot \nabla_{\theta_m^k} L_{m,a}^k - \eta_2 \cdot \nabla_{\theta_m^k} L_s^k$ 
39:      $\phi_m^{k+1} \leftarrow \phi_m^k - \gamma_1 \cdot \nabla_{\phi_m^k} L_{m,a}^k - \gamma_2 \nabla_{\phi_m^k} L_s^k$ 
40:   end for
41: end while

```

15 PROOFS

15.1 DERIVATIVES OF L_s WITH RESPECT TO CLIENT PARAMETERS θ_m AND ϕ_m

Proposition 15.1. *Using the chain rule, the derivatives of the server loss L_s with respect to the augmented client parameters of client m (i.e., ϕ_m and θ_m) are*

$$\nabla_{\theta_m} L_s = \sum_{t=1}^T (A_{mm}^\top \nabla_{h_{m,a}^t} L_s + \nabla_{\hat{h}_{m,a}^{t-1}} L_s) y_m^{t-1\top}, \quad (26)$$

$$\nabla_{\phi_m} L_s = \sum_{t=1}^T \nabla_{h_{m,a}^t} L_s. \quad (27)$$

Proof. From the model,

$$h_{m,a}^t = A_{mm} \hat{h}_{m,a}^{t-1} + b_m^{t-1} + \phi_m, \quad \hat{h}_{m,a}^{t-1} = c_m^{t-1} + \theta_m y_m^{t-1}.$$

To make the chain rule bookkeeping explicit, consider the proxy loss

$$\ell(h^t, \hat{h}^{t-1}) := \frac{1}{T} \sum_{t=1}^T \left(\|h^t - X^t\|_2^2 + \xi \|A\hat{h}^{t-1} - Z^{t-1}\|_2^2 \right),$$

with the same computational graph

$$h^t = A\hat{h}^{t-1} + b^{t-1} + \phi, \quad \hat{h}^{t-1} = c^{t-1} + \theta y^{t-1}.$$

We use Einstein summation over repeated Latin indices. Indices $p, k, r \in \{1, \dots, P\}$ denote state components and $j, s \in \{1, \dots, D\}$ denote measurement components. The Kronecker delta is δ_{ij} , and subscripts on a vector/matrix denote components.

Derivative with respect to θ . By the chain rule,

$$\frac{\partial \ell}{\partial \theta_{rs}} = \frac{1}{T} \sum_{t=1}^T \sum_{p=1}^P \left(\frac{\partial \ell}{\partial h_p^t} \frac{\partial h_p^t}{\partial \theta_{rs}} + \frac{\partial \ell}{\partial \hat{h}_p^{t-1}} \frac{\partial \hat{h}_p^{t-1}}{\partial \theta_{rs}} \right).$$

From $h_p^t = A_{pk} \hat{h}_k^{t-1} + b_p^{t-1} + \phi_p$ and $\hat{h}_k^{t-1} = c_k^{t-1} + \theta_{kj} y_j^{t-1}$,

$$\frac{\partial \hat{h}_k^{t-1}}{\partial \theta_{rs}} = \delta_{kr} y_s^{t-1}, \quad \frac{\partial h_p^t}{\partial \theta_{rs}} = A_{pk} \frac{\partial \hat{h}_k^{t-1}}{\partial \theta_{rs}} = A_{pk} \delta_{kr} y_s^{t-1} = A_{pr} y_s^{t-1}.$$

Hence,

$$\begin{aligned} \frac{\partial \ell}{\partial \theta_{rs}} &= \frac{1}{T} \sum_{t=1}^T \left[\left(\frac{\partial \ell}{\partial h_p^t} \right) A_{pr} + \left(\frac{\partial \ell}{\partial \hat{h}_p^{t-1}} \right) \delta_{pr} \right] y_s^{t-1} \\ &= \frac{1}{T} \sum_{t=1}^T \left[(A^\top \nabla_{h^t} \ell)_r + (\nabla_{\hat{h}^{t-1}} \ell)_r \right] y_s^{t-1}. \end{aligned}$$

Collecting the (r, s) -entries, the matrix form is

$$\nabla_{\theta} \ell = \frac{1}{T} \sum_{t=1}^T (A^\top \nabla_{h^t} \ell + \nabla_{\hat{h}^{t-1}} \ell) (y^{t-1})^\top.$$

Derivative with respect to ϕ . Again by the chain rule,

$$\frac{\partial \ell}{\partial \phi_a} = \frac{1}{T} \sum_{t=1}^T \sum_{p=1}^P \frac{\partial \ell}{\partial h_p^t} \frac{\partial h_p^t}{\partial \phi_a} = \frac{1}{T} \sum_{t=1}^T \sum_{p=1}^P \frac{\partial \ell}{\partial h_p^t} \delta_{pa} = \frac{1}{T} \sum_{t=1}^T [\nabla_{h^t} \ell]_a,$$

or, in matrix form,

$$\nabla_{\phi} \ell = \frac{1}{T} \sum_{t=1}^T \nabla_{h^t} \ell.$$

Finally, reinstating the client- m notation

$$A \mapsto A_{mm}, \quad h^t \mapsto h_{m,a}^t, \quad \hat{h}^{t-1} \mapsto \hat{h}_{m,a}^{t-1}, \quad y^{t-1} \mapsto y_m^{t-1},$$

and replacing ℓ by L_s (the factor $1/T$ is an inconsequential constant), yields

$$\nabla_{\theta_m} L_s = \sum_{t=1}^T (A_{mm}^\top \nabla_{h_{m,a}^t} L_s + \nabla_{\hat{h}_{m,a}^{t-1}} L_s) y_m^{t-1\top}, \quad \nabla_{\phi_m} L_s = \sum_{t=1}^T \nabla_{h_{m,a}^t} L_s,$$

as claimed. □

15.2 PROPOSITION 4.1

Proof. Consider the LTI system without a direct term:

$$h^t = Ah^{t-1} + Bu^{t-1} + w^{t-1}, \quad y^t = Ch^t + v^t,$$

with $w^{t-1} \sim \mathcal{N}(0, Q)$, $v^t \sim \mathcal{N}(0, R)$, independent.

(1) Abduction. Let \mathcal{Y}_{t-1} denote data up to $t-1$. The Kalman filter yields

$$h^{t-1} \mid \mathcal{Y}_{t-1} \sim \mathcal{N}(\hat{h}^{t-1}, P^{t-1|t-1}).$$

Carry this posterior (and noise laws) unchanged into the counterfactual.

(2) Action. Apply the intervention $\text{do}(u^{t-1} = u)$: replace u^{t-1} by the chosen constant u in the state update; all other mechanisms unchanged.

(3) Prediction. Under the intervention (action) represented by $\text{do}(u^{t-1} = u)$ we have,

$$h^t \mid \mathcal{Y}_{t-1} \sim \mathcal{N}(A\hat{h}^{t-1} + Bu, P^{t|t-1}), \quad P^{t|t-1} = AP^{t-1|t-1}A^\top + Q,$$

and hence

$$y^t \mid \text{do}(u^{t-1} = u), \mathcal{Y}_{t-1} \sim \mathcal{N}(\mu(u), S_t), \quad \mu(u) := C(A\hat{h}^{t-1} + Bu), \quad S_t := CP^{t|t-1}C^\top + R.$$

Therefore, for u_0, u_1 ,

$$\mu(u_1) - \mu(u_0) = CB(u_1 - u_0), \quad S_t \text{ is identical.}$$

Hence we directly obtain *ATE* as follows,

$$\text{ATE} = \mathbb{E}[y^t \mid \text{do}(u_1)] - \mathbb{E}[y^t \mid \text{do}(u_0)] = CB(u_1 - u_0).$$

□

15.3 THEOREM 6.1

Proof. For any $m \in \{1, \dots, M\}$, define

$$x_m^t := \sum_{n \neq m} \hat{A}_{mn} \hat{h}_{n,c}^t, \quad r_m^t := h_{a,m}^t - A_{mm} \hat{h}_{m,c}^t - B_{mm} u_m^t - \sum_{n \neq m} \hat{B}_{mn} u_n^t, \quad z_m^t := A_{mm} (\hat{h}_{a,m}^t - \hat{h}_{m,c}^t).$$

The per-time server loss in the A -block is

$$L_s^t = \|r_m^t - x_m^t\|_2^2 + \xi \|z_m^t - x_m^t\|_2^2.$$

Since L_s^t depends on $\{\hat{A}_{mn}\}$ only through x_m^t , by the chain rule

$$\nabla_{\hat{A}_{mn}} L_s^t = (\nabla_{x_m^t} L_s^t) (\hat{h}_{n,c}^t)^\top, \quad \nabla_{x_m^t} L_s^t = 2[(1 + \xi)x_m^t - (r_m^t + \xi z_m^t)].$$

Training minimizes the time-average $\frac{1}{T} \sum_{t=1}^T L_s^t$, hence at a stationary point

$$\frac{1}{T} \sum_{t=1}^T \nabla_{x_m^t} L_s^t = 0 \implies \frac{1}{T} \sum_{t=1}^T [(1 + \xi)x_m^t - (r_m^t + \xi z_m^t)] = 0.$$

By the ergodicity assumption, time averages converge to expectations, so

$$(1 + \xi) \mathbb{E}[x_m^t] = \mathbb{E}[r_m^t] + \xi \mathbb{E}[z_m^t].$$

Letting $\xi \rightarrow \infty$ yields

$$\mathbb{E}[x_m^t] = \mathbb{E}[z_m^t].$$

Finally, by augmentation $\hat{h}_{a,m}^t = \hat{h}_{m,c}^t + \theta_m^* y_m^t$, so

$$z_m^t = A_{mm} \theta_m^* y_m^t, \quad x_m^t = \sum_{n \neq m} \hat{A}_{mn}^* \hat{h}_{n,c}^t,$$

and therefore

$$\mathbb{E}[A_{mm} \theta_m^* y_m^t] = \mathbb{E}\left[\sum_{n \neq m} \hat{A}_{mn}^* \hat{h}_{n,c}^t\right].$$

□

15.4 COROLLARY 6.2

Proof. For any client m , we define,

$$p_m^t := \sum_{n \neq m} \hat{B}_{mn} u_n^t, \quad c_m^t := h_{a,m}^t - A_{mm} \hat{h}_{m,c}^t - B_{mm} u_m^t.$$

With x_m^t fixed, the per-time loss in the B -block is

$$L_s^t(p_m^t) = \|c_m^t - x_m^t - p_m^t\|_2^2 + \xi \|z_m^t - x_m^t\|_2^2,$$

so

$$\nabla_{p_m^t} L_s^t = -2(c_m^t - x_m^t - p_m^t).$$

Stationarity of the time-average gives

$$\frac{1}{T} \sum_{t=1}^T \nabla_{p_m^t} L_s^t = 0 \implies \frac{1}{T} \sum_{t=1}^T (c_m^t - x_m^t - p_m^t) = 0.$$

By ergodicity,

$$\mathbb{E}[p_m^t] = \mathbb{E}[c_m^t - x_m^t].$$

From Theorem 6.1, as $\xi \rightarrow \infty$, $\mathbb{E}[x_m^t] = \mathbb{E}[z_m^t] = \mathbb{E}[A_{mm}(\hat{h}_{a,m}^t - \hat{h}_{m,c}^t)]$, hence

$$\mathbb{E}[c_m^t - x_m^t] = \mathbb{E}[h_{a,m}^t - A_{mm}\hat{h}_{m,c}^t - B_{mm}u_m^t - A_{mm}(\hat{h}_{a,m}^t - \hat{h}_{m,c}^t)] = \mathbb{E}[h_{a,m}^t - A_{mm}\hat{h}_{a,m}^t - B_{mm}u_m^t].$$

Using the augmented client model $h_{a,m}^t = A_{mm}\hat{h}_{a,m}^t + B_{mm}u_m^t + \phi_m^*$ at stationarity yields

$$\mathbb{E}[c_m^t - x_m^t] = \mathbb{E}[\phi_m^*] = \phi_m^*,$$

so

$$\phi_m^* = \mathbb{E}[p_m^t] = \mathbb{E}\left[\sum_{n \neq m} \hat{B}_{mn}^* u_n^t\right].$$

□

15.5 LEMMA 7.2

Proof. Since $L_{m,a} = \frac{1}{T} \sum_{t=1}^T \|r_{m,a}^t\|^2$, its gradients are given as:

$$\begin{aligned} \nabla_{\theta_m} L_{m,a} &= -\frac{2}{T} \sum_{t=1}^T (C_{mm}A_{mm})^\top r_{m,a}^t (y_m^{t-1})^\top, \\ \nabla_{\phi_m} L_{m,a} &= -\frac{2}{T} \sum_{t=1}^T C_{mm}^\top r_{m,a}^t. \end{aligned}$$

At a stationary point, $\nabla_{\theta_m} L_{m,a} = 0$ and $\nabla_{\phi_m} L_{m,a} = 0$, hence

$$\frac{1}{T} \sum_{t=1}^T (C_{mm}A_{mm})^\top r_{m,a}^{*,t} (y_m^{t-1})^\top = 0, \quad \frac{1}{T} \sum_{t=1}^T C_{mm}^\top r_{m,a}^{*,t} = 0.$$

By the ergodicity assumption, these time-averages converge to expectations, giving

$$\mathbb{E}[(C_{mm}A_{mm})^\top r_{m,a}^{*,t} (y_m^{t-1})^\top] = 0, \quad \text{and} \quad \mathbb{E}[C_{mm}^\top r_{m,a}^{*,t}] = 0.$$

□

15.6 THEOREM 7.3

Proof. From the augmented client model, we write $\tilde{y}_{m,a}^t$ as

$$\begin{aligned} h_{m,a}^t &= A_{mm}(\hat{h}_{m,c}^{t-1} + \theta_m^* y_m^{t-1}) + B_{mm}u_m^{t-1} + \phi_m^*, \\ \tilde{y}_{m,a}^t(\theta_m^*, \phi_m^*) &= C_{mm}h_{m,a}^t \\ &= C_{mm}A_{mm}\theta_m^* y_m^{t-1} + C_{mm}A_{mm}\hat{h}_{m,c}^{t-1} + C_{mm}B_{mm}u_m^{t-1} + C_{mm}\phi_m^*. \end{aligned}$$

Adding and subtracting the cross-input block so that all inputs $u^{t-1} = [u_1^{t-1}; \dots; u_M^{t-1}]$ appear linearly:

$$\begin{aligned} \tilde{y}_{m,a}^t(\theta_m^*, \phi_m^*) &= C_{mm}A_{mm}\theta_m^* y_m^{t-1} + C_{mm}[\hat{B}_{m1}^*, \dots, B_{mm}, \dots, \hat{B}_{mM}^*] u^{t-1} + C_{mm}A_{mm}\hat{h}_{m,c}^{t-1} \\ &\quad + C_{mm}\left(\phi_m^* - \sum_{n \neq m} \hat{B}_{mn}^* u_n^{t-1}\right). \end{aligned}$$

Define the stacked regressor and the coefficient matrix

$$z_m^{t-1} := \begin{bmatrix} y_m^{t-1} \\ u^{t-1} \\ \hat{h}_{m,c}^{t-1} \end{bmatrix}, \quad M_{\text{fed}} := \begin{bmatrix} C_{mm}A_{mm}\theta_m^* & C_{mm}[\hat{B}_{m1}^*, \dots, B_{mm}, \dots, \hat{B}_{mM}^*] & C_{mm}A_{mm} \end{bmatrix},$$

and the zero-mean error e_t as,

$$e_t := C_{mm} \left(\phi_m^* - \sum_{n \neq m} \hat{B}_{mn}^* u_n^{t-1} \right), \quad \mathbb{E}[e_t] = 0 \text{ (by Corollary 6.2).}$$

Then we have this affine relationship,

$$\tilde{y}_{m,a}^t(\theta_m^*, \phi_m^*) = M_{\text{fed}} z_m^{t-1} + e_t.$$

From the theorem, we know that $\Sigma_z := \mathbb{E}[z_m^{t-1} z_m^{t-1\top}]$ and $\Gamma_{yz} := \mathbb{E}[y_m^t z_m^{t-1\top}]$. Using Lemma 7.2 we have,

$$\mathbb{E}[(C_{mm} A_{mm})^\top r_{m,a}^{*,t} (y_m^{t-1})^\top] = 0, \quad \mathbb{E}[C_{mm}^\top r_{m,a}^{*,t}] = 0.$$

Since $C_{mm} A_{mm}$ is full column rank, there exists a left inverse L_{mm} with $L_{mm} (C_{mm} A_{mm}) = I$, so

$$\mathbb{E}[r_{m,a}^{*,t} (y_m^{t-1})^\top] = 0.$$

Stacking with the input and state–estimate blocks gives

$$\mathbb{E}[(y_m^t - \tilde{y}_{m,a}^t) z_m^{t-1\top}] = [0, \mathbb{E}[r_{m,a}^{*,t} (u^{t-1})^\top], \mathbb{E}[r_{m,a}^{*,t} (\hat{h}_{m,c}^{t-1})^\top]].$$

Substitute $\tilde{y}_{m,a}^t = M_{\text{fed}} z_m^{t-1} + e_t$ to obtain

$$\Gamma_{yz} - M_{\text{fed}} \Sigma_z - \mathbb{E}[e_t z_m^{t-1\top}] = [0, \mathbb{E}[r_{m,a}^{*,t} (u^{t-1})^\top], \mathbb{E}[r_{m,a}^{*,t} (\hat{h}_{m,c}^{t-1})^\top]].$$

Now use $r_{m,a}^{*,t} := y_m^t - y_{m,a}^t = y_m^t - (M_{\text{fed}} z_m^{t-1} + e_t)$ to rewrite the two nonzero blocks:

$$\mathbb{E}[r_{m,a}^{*,t} (u^{t-1})^\top] = \mathbb{E}[(y_m^t - M_{\text{fed}} z_m^{t-1}) (u^{t-1})^\top] - \mathbb{E}[e_t (u^{t-1})^\top],$$

and similarly

$$\mathbb{E}[r_{m,a}^{*,t} (\hat{h}_{m,c}^{t-1})^\top] = \mathbb{E}[(y_m^t - M_{\text{fed}} z_m^{t-1}) (\hat{h}_{m,c}^{t-1})^\top] - \mathbb{E}[e_t (\hat{h}_{m,c}^{t-1})^\top].$$

But the first terms on the right in these two lines are exactly the u - and \hat{h} -blocks of $(\Gamma_{yz} - M_{\text{fed}} \Sigma_z)$. Therefore the whole right-hand side equals $(\Gamma_{yz} - M_{\text{fed}} \Sigma_z) - \mathbb{E}[e_t z_m^{t-1\top}]$, and we conclude

$$\Gamma_{yz} - M_{\text{fed}} \Sigma_z - \mathbb{E}[e_t z_m^{t-1\top}] = 0.$$

hence we obtain,

$$M_{\text{fed}} = \Gamma_{yz} \Sigma_z^{-1} - \mathbb{E}[e_t z_m^{t-1\top}] \Sigma_z^{-1}.$$

Define the oracle (centralized model) linear predictor on the same regressors:

$$\tilde{y}_{m,o}^t := M_o z_m^{t-1}, \quad M_o := \Gamma_{yz} \Sigma_z^{-1}.$$

Therefore

$$\tilde{y}_{m,o}^t - \tilde{y}_{m,a}^t(\theta_m^*, \phi_m^*) = (M_o - M_{\text{fed}}) z_m^{t-1} - e_t = \underbrace{\mathbb{E}[e_t z_m^{t-1\top}] \Sigma_z^{-1}}_{=: J_m} z_m^{t-1} - e_t.$$

Taking expectations and using $\mathbb{E}[e_t] = 0$ gives the claimed relation

$$\mathbb{E}[\tilde{y}_{m,o}^t - \tilde{y}_{m,a}^t(\theta_m^*, \phi_m^*)] = J_m \mathbb{E}[z_m^{t-1}].$$

□

15.7 LEMMA A.6

Proof. By definition, $z_m^t = [\hat{h}_{m,c}^t; \hat{h}_{m,a}^t; h_{m,a}^t; u_m^t]$ with the same u_m^t in \mathcal{D}_m and \mathcal{D}'_m . Thus,

$$\|z_m^t - z_m^{t'}\|_2 \leq \|\hat{h}_{m,c}^t - \hat{h}_{m,c}^{t'}\|_2 + \|\hat{h}_{m,a}^t - \hat{h}_{m,a}^{t'}\|_2 + \|h_{m,a}^t - h_{m,a}^{t'}\|_2.$$

Contractivity implies that a one-time perturbation at $y_m^{t^*}$ of magnitude at most $R_y \leq R_{\max}$ yields

$$\|h_{m,a}^t - h_{m,a}^{t'}\|_2 \leq L_m \beta_m^{t-t^*} R_{\max} \quad (t \geq t^*),$$

Collecting constants from the observer/augmenter maps and using subadditivity of $\|\cdot\|_2$, there exists a finite κ_m (depending on L_m, β_m and the estimator gains) such that

$$\|z_m^t - z_m^{t'}\|_2 \leq \kappa_m R_{\max}.$$

One we have the above inequality, we define $\Delta_{m,\text{msg}} := \kappa_m R_{\max}$. \square

15.8 LEMMA A.8

Proof. For notational brevity we write,

$$H_m^t := A_{mm} \hat{h}_{m,c}^{t-1} + \sum_{n \neq m} \hat{A}_{mn} \hat{h}_{n,c}^{t-1} + B_{mm} u_m^{t-1} + \sum_{n \neq m} \hat{B}_{mn} u_n^{t-1}$$

Thus, the server gradient expression is now given as,

$$g_m^t = \frac{2}{T} (h_{m,a}^t - H_m^t).$$

Hence we obtain,

$$\|g_m^t - g_m^{t'}\|_2 \leq \frac{2}{T} (\|h_{m,a}^t - h_{m,a}^{t'}\|_2 + \|H_m^t - H_m^{t'}\|_2).$$

(i) *First term:* a one-time change in $y_{m'}^{t^*}$ propagates to $h_{m',a}^t$ using $\|h_{m',a}^t - h_{m',a}^{t'}\|_2 \leq L_{m'} \beta_{m'}^{t-t^*} R_{\max}$. This yields the contribution $L_{m'} \|C_{mm}\| \beta_{m'}^{t-t^*} R_{\max}$.

(ii) *Second term:* For $n \neq m$, $\|\hat{h}_{n,c}^{t-1} - \hat{h}_{n,c}^{t-1'}\|_2 \leq L_n \beta_n^{t-1-t^*} R_{\max}$ if $n = m'$ and zero otherwise (each client's proprietary estimator depends only on its own measurements). Thus we obtain,

$$\|H_m^t - H_m^{t'}\|_2 \leq \sum_{n \neq m} \|\hat{A}_{mn}\| \|\hat{h}_{n,c}^{t-1} - \hat{h}_{n,c}^{t-1'}\|_2 \leq \sum_{n \neq m} \|\hat{A}_{mn}\| L_n \beta_n^{t-1-t^*} R_{\max}.$$

Combining (i) and (ii), absorbing $\beta_n^{t-1-t^*} \leq \beta_n^{t-t^*}$ and multiplying by the prefactor $\frac{2}{T}$ plus the linear factor $(1 + \|A_{mm}\|)$ from the residual structure yields

$$\|g_m^t - g_m^{t'}\|_2 \leq \frac{2}{T} (1 + \|A_{mm}\|) L_{m'} \left(\|C_{mm}\| + \sum_{n \neq m} \|A_{mn}\| \beta_n^{t-t^*} \right) R_{\max}.$$

Adding $\sum_{n \neq m} \|B_{mn}\|$ inside the bracket gives a looser but still valid bound; this produces exactly the stated $\kappa_{m,\text{mix}}$. \square

15.9 PROPOSITION A.11

Proof. Consider a mechanism with ℓ_2 -sensitivity Δ and clipping C s.t., $\tilde{x} = \mathcal{M}(x) + \mathcal{N}(0, \sigma^2 C^2 I)$. For neighboring inputs x, x' , the privacy loss random variable is Gaussian-subgaussian; the classical analysis of the (basic) Gaussian mechanism yields

$$\sigma \geq \frac{\Delta}{C} \cdot \frac{\sqrt{2 \ln(1.25/\delta)}}{\varepsilon}$$

as a sufficient condition for (ε, δ) -DP.

Applying this with $(\Delta, C) = (\Delta_{m,\text{msg}}, C_{\text{msg}})$ for messages and $(\Delta_{m,\text{grad}}, C_{\text{grad}})$ for gradients gives the two stated inequalities. \square

15.10 PROPOSITION A.12

Proof. (Sequential composition.) If \mathcal{M}_1 is $(\varepsilon_1, \delta_1)$ -DP and \mathcal{M}_2 is $(\varepsilon_2, \delta_2)$ -DP, then the pair $(\mathcal{M}_1, \mathcal{M}_2)$ is $(\varepsilon_1 + \varepsilon_2, \delta_1 + \delta_2)$ -DP by the standard composition theorem (union bound on failure events and multiplicativity of the likelihood ratio bounds). Inducting over R rounds yields $(\sum_r \varepsilon_r, \sum_r \delta_r)$.

(Joint per-round composition.) In each round, releasing both message and gradient corresponds to composing two mechanisms with guarantees $(\varepsilon_{\text{msg}}, \delta_{\text{msg}})$ and $(\varepsilon_{\text{grad}}, \delta_{\text{grad}})$, so the per-round guarantee is $(\varepsilon_{\text{msg}} + \varepsilon_{\text{grad}}, \delta_{\text{msg}} + \delta_{\text{grad}})$. Composing these R times proves the stated bound. \square

15.11 COROLLARY A.13

Proof. Let \mathcal{M} denote the overall privatized training mechanism that produces the transcript $\mathcal{T}_{\text{priv}} = \{\tilde{z}_m^t, \tilde{g}_m^t\}_{m,t}$. We know that, \mathcal{M} satisfies (ε, δ) -differential privacy with respect to the raw measurement $\mathcal{D} = \{y_m^t\}$.

After the privatized transcript is generated, all subsequent computations, including optimization of system matrices $\{\hat{A}_{mn}, \hat{B}_{mn}\}$, client updates of $\{\theta_m, \phi_m\}$, and downstream counterfactual predictions are deterministic or randomized functions of $\mathcal{T}_{\text{priv}}$ only. Let us denote this transformation by

$$\mathcal{T}_{\text{post}} : \mathcal{T}_{\text{priv}} \mapsto (\hat{A}, \hat{B}, \theta, \phi, \widehat{\text{ATE}}, \widehat{\text{CF}}).$$

For any pair of neighboring datasets $\mathcal{D}, \mathcal{D}'$ that differ in one measurement $y_{m^*}^{t^*}$, the privacy guarantee of \mathcal{M} implies that for every measurable set S ,

$$\Pr[\mathcal{M}(\mathcal{D}) \in S] \leq e^\varepsilon \Pr[\mathcal{M}(\mathcal{D}') \in S] + \delta.$$

Because $\mathcal{T}_{\text{post}}$ is applied only to the outputs of \mathcal{M} , we can substitute $S' = \mathcal{T}_{\text{post}}^{-1}(S)$ to obtain

$$\Pr[\mathcal{T}_{\text{post}} \circ \mathcal{M}(\mathcal{D}) \in S] = \Pr[\mathcal{M}(\mathcal{D}) \in S'] \leq e^\varepsilon \Pr[\mathcal{M}(\mathcal{D}') \in S'] + \delta = e^\varepsilon \Pr[\mathcal{T}_{\text{post}} \circ \mathcal{M}(\mathcal{D}') \in S] + \delta.$$

Hence $\mathcal{T}_{\text{post}} \circ \mathcal{M}$ is also (ε, δ) -DP. \square